A Case for an Ultra Massive Black Hole in the Galaxy Cluster MS0735.6+7421

by

Razzi Movassaghi Jorshari
B.Sc., Sharif University of Technology, 2008

A Thesis Submitted in Partial Fulfillment of the
Requirements for the Degree of

MASTER OF SCIENCE

in the Department of Physics & Astronomy

A Case for an Ultra Massive Black Hole in the Galaxy Cluster MS0735.6+7421

by

Razzi Movassaghi Jorshari
B.Sc., Sharif University of Technology, 2008

Supervisory Committee

Dr. Arif Babul, Supervisor
(Department of Physics & Astronomy)

Dr. Chris Pritchet, Departmental Member
(Department of Physics & Astronomy)

Dr. Rogerio de Sousa, Departmental Member
(Department of Physics & Astronomy)

Supervisory Committee

Dr. Arif Babul, Supervisor
(Department of Physics & Astronomy)

Dr. Chris Pritchet, Departmental Member
(Department of Physics & Astronomy)

Dr. Rogerio de Sousa, Departmental Member
(Department of Physics & Astronomy)

ABSTRACT

In this work, we study the galaxy cluster MS0735.6+7421 that hosts the most energetic observed active galactic nucleus (AGN) outburst so far. Explaining this very energetic AGN outburst is found to be challenging. McNamara et al. (2009) grappled with this problem and proposed two possible solutions: either the black hole (BH) must be an ultra massive one (with mass $> 10^{10}$ $M_{\odot}$), or the efficiency of the mass to energy conversion (ϵ) should be higher than the generally assumed value of $\epsilon \sim 0.1$. However, the efficiency of the mass to energy conversion depends on the BH's spin (Benson & Babul, 2009); higher ϵ can be achieved with a higher spinning BH. Here, we explore the second solution in detail, and ask the question: How did the BH spin up to the very high spins in advance of the outburst? We also explore the attendant physical processes, such as star formation, during the spin-up mode and investigate the associated observational implications. Comparing our results with what is generally expected from simulations and observational studies suggests that for all intents and purposes, the existence of an ultra massive BH is the simplest solution.

Contents

List of Figures

Acknowledgements

I would like to thank:

My supervisor, Dr. Arif Babul,
My supervisory committee,
My first graduate advisor at UVic, Dr. Michel Lefebvre,
All the office staff in the Physics & Astronomy department of UVic,
All the faculty members in the Physics & Astronomy department of UVic,
All the astrograds at UVic, particularly Chris Bildfell, Hannah Broekhoven-Fiene, and Charli Sakari,
and last but not least, all my friends in Victoria & Vancouver.

This work could not have been done without your help and support.

Dedication

To my parents, for their endless love and support.

Chapter 1

Introduction

A galaxy is a gravitationally bound system of stars, stellar remnants, gas, dust, and dark matter. Different galaxies have different characteristics, and can be categorized according to their morphology, spectral features, mass, luminosity and etc. While stellar luminosity is one of the main parameters to investigate galaxy formation and evolution, there are some galaxies with significantly high luminosities emitted from the central regions which cannot be explained by only a stellar component. These extremely bright central regions are known as *active galactic nuclei* (AGNs). It is believed that accretion of matter onto a massive black hole (BH) at the center of the galaxy could power these extremely luminous objects. The importance of such a phenomenon in the galaxy evolution has been studied (e.g. Burbidge et al., 1963), and more efforts have been made recently to understand the nature and properties of AGNs.

1.1 Historical Review

The very first observation of an AGN took place accidentally by Fath (1909). At that time, no one was aware of the existence of AGN. Fath was investigating whether "spiral nebulae" were an unresolved collection of stars or just gaseous objects. He did it by looking at the spectra of those systems. He reported that most of his objects had a continuous spectrum with absorption lines. A continuous spectrum is a spectrum in which the radiation is distributed over all frequencies, not just a few specific frequency ranges. A prime example is the black-body radiation emitted by a hot, dense body. Moreover, an absorption line will appear in a spectrum if an absorbing material is

placed between a source and the observer. This material could be the outer layers of a star, a cloud of interstellar gas or a cloud of dust. Therefore, he argued that most of his objects were consistent with the former scenario, and they could be considered as a stellar population surrounding by cool gas. For NGC 1068, however, he observed a combination of both absorption and emission lines. Emission lines were also observed in gaseous nebulae which implied that hot excited gas should be present in NGC 1068.

Later works by Slipher (1917) and Hubble (1926) confirmed the existence of nuclear emission lines in the spectra of these galaxies, and also noted a "width" of the emission line that could be interpreted as the effect of having a radial velocity towards/away from Earth. This effect is also known as Doppler shifting. However, the first serious study about these objects was done by Seyfert (1943). He studied a group of high central surface brightness galaxies and realized that high-excitation nuclear emission lines dominated the optical spectra of several galaxies. These emission lines require gas to be excited by a very energetic source. He also found large widths of emission lines that corresponded to Doppler shifts on the order of a few thousand of km s^{-1}.

Later studies showed that these types of galaxies, which have been named Seyfert Galaxies, can be generally categorized into two classes. Seyfert Type 1 galaxies are the ones with both broad (high Doppler shifting) and narrow (low Doppler shifting) emission lines in their spectra. The presence of X-ray and weak radio emission are other features of this type. It has also been found that this type of galaxy shows variation in brightness. On the other hand, Seyfert type 2 galaxies only have narrow emission lines. They also have weak radio and X-ray emission, and are not variable. Seyferts are usually found to be spiral galaxies. Although these types of AGN have been named after Seyfert, his pioneer work at the time was not enough to encourage astronomers to investigate AGN. Serious investigations and studies started in the epoch of "radio astronomy".

After World War II, due to improvements in radio engineering, several radio surveys of galaxies were conducted by different groups. The Third Cambridge (3C) catalog (Edge et al., 1959), 3CR catalog (Bennett, 1962), PKS (Ekers, 1969), 4C (Pilkington & Scott, 1965; Gower et al., 1967), AO (Hazard et al., 1967) and Ohio (Ehman et al., 1970) were part of the important early surveys. These surveys observed galaxies with characteristics different from normal ones. They were extremely bright at radio wavelengths and were therefore called "radio galaxies". Similar to Seyfert

galaxies, they were later divided into two types: broad-line radio galaxies (BLRGs) and narrow-line radio galaxies (NLRGs). BLRGs have both broad and narrow emission lines, and emit strong radio emission. These galaxies are also variable, and show weak polarization[1]. NLRGs only have narrow emission lines. They also have strong radio emission, but no polarization and no variability. Both BLRGs and NLRGs are usually found in elliptical galaxies.

Finding BLRGs and NLRGs was not the only achievement of radio surveys. By that time, astronomers were able to identify the position of radio sources. Most of these sources matched the position of a previously observed galaxies, but some positions were coincident with "star-like objects" (Matthews & Sandage, 1963; Hazard et al., 1963). The nature of these "radio stars" or "quasi stellar radio sources" (quasars) was unknown, and their extremely high luminosities required a new physical mechanism to explain them. Soon after, a possible explanation for these objects was suggested: a massive black hole at the centre of the galaxy that accretes material from the galaxy (Zel'Dovich, 1965) . The importance of such a phenomenon in galaxy formation and evolution was also investigated (e.g Burbidge et al., 1963). Furthermore, quasars could be potential candidates for cosmological probes at large distances because of their extremely high luminosity. For all these reasons, studying quasars became a major focus for astronomers. Quasars have been found to have two different types: radio-loud (QSR) and radio quiet (QSO). Both types have broad and narrow emission lines, and are variable. However, QSRs have strong radio emission and some polarization, while QSOs have weak radio emission and weak polarization.

Further works found different types of galaxies, which could all be categorized as different types of AGN. Blazars are a kind of AGN that exhibit rapid variability and strong polarization. A subclass of Blazars is BL Lac objects. Besides the above mentioned characteristics for Blazars, they also show strong radio emission, and are almost devoid of emission lines. BL Lacs are mostly elliptical galaxies. Another subclass of Blazars is OVV quasars. These objects have both broad and narrow lines, and emit strong radio emission. They are also found to be much more luminous than BL Lacs.

There are other types of galaxies which can be categorized as AGNs, though other origins could also explain their features. Ultraluminous infrared galaxies (ULIRGs)

[1]Polarization is a property of light that describes the orientation of its oscillations and can give some information about the light source. Ordinary light from sources such as the Sun contains light of all different polarizations.

are one of those groups. While some astronomers believe that they are starburst galaxies (galaxies in which a very large number of stars have recently formed), others suggest these galaxies are quasars which have been enshrouded in dust. The infrared light would then be a result of absorption and re-radiation of the quasar nucleus light by dust. Another group is Low Ionization Nuclear Emission-line Regions (LINERs). While these objects have similar features as low-luminosity Seyfert Type 2 galaxies and have low-ionization emission lines in their spectra, they might also be starburst galaxies or H II regions (regions of ionized hydrogen around a hot star).

1.2 An Explanation for AGN

As has been mentioned, the engine of the AGNs is believed to be the mass accretion onto a super massive black hole (SMBH) at the center of the galaxy. Figure 1.1 shows a schematic cartoon that illustrates the accepted picture of the central region of a galaxy with an AGN. One of the main parameters that determines the type of the AGN activity is the structure of the accretion flow onto the SMBH. However, the structure of the accretion flow depends on the accretion rate of the flow. There is a critical accretion rate that determines different accretion structures. This critical rate is found to be 0.01 of the Eddington limit. The Eddington limit is the point when the inward gravitational force is equal to the outward force of the radiation. For lower accretion rates than 0.01 of the Eddington limit, the flow is an advection-dominated accretion mode and is geometrically thick (Narayan & Yi, 1995). For higher accretion rates, the accretion flow forms a thin disk around the BH. However, one should note that for very high accretion rates ($\gtrsim 0.1$ of Eddington limit), the structure of the flow becomes geometrically thick again.

When the BH accretes via a thin disk, material in the accretion disk loses its angular momentum due to viscosity or other turbulent processes which causes the accretion disk to heat up. Generally, accretion can be very efficient in converting potential and kinetic energy into heat and radiation. Radiation from an accretion disk produces a continuous spectrum that peaks at optical-ultraviolet wavelengths. In the inner regions of the accretion disk, material orbits the BH at very high angular frequencies (high velocities) which makes it possible to radiate soft (low-energy) X-rays. Moreover, inverse Compton scattering with hot and relativistic electrons above the disk can scatter photons to much higher energies and produce hard X-ray photons. Also, part of the observed X-ray spectrum is produced by the thermal bremsstrahlung

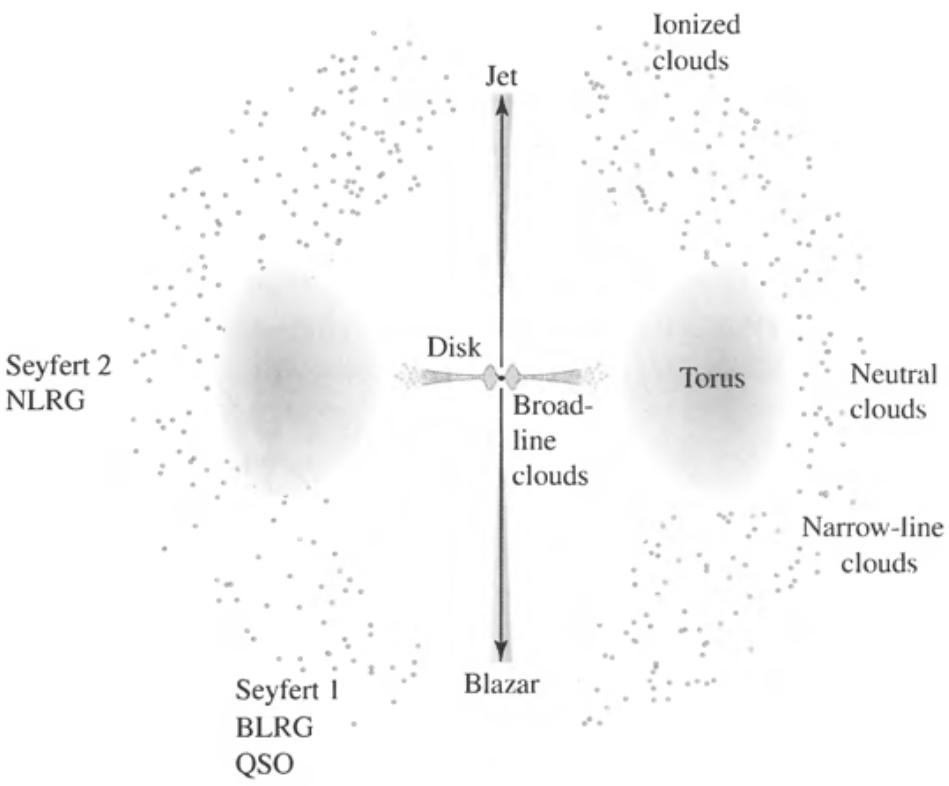

Figure 1.1 The schematic cartoon of the central region of a galaxy hosting AGN. Different regions are displayed. The figure shows how various viewing angles can result in observations of different types of AGN. This figure is reprinted from Carroll & Ostlie (2007).

mechanism. Bremsstrahlung, also known as free-free, radiation is the mechanism of producing electromagnetic radiation when a charged particle is deflected and decelerated by another charged particle.

Material close to the BH, excited by the radiation from the accretion disk, can radiate at specific wavelengths and produce the observed emission lines in the spectrum of the AGN. Relatively close to the BH, there is a region called the "broad-line region" which contains clumpy clouds of partially ionized gas that are moving rapidly in the BH's potential well. These "broad-line clouds" are responsible for the broad strong optical and ultraviolet emission lines observed in Seyfert Type 1s, quasars, BLRGs, etc. Outside the accretion disk and broad-line region, there is an optically thick torus of gas and dust that can obscure the inner continuum and emission-line radiation along some lines of sight. This can explain the absence of broad-line emission in the spectrum of some types of AGNs, e.g. Seyfert 2 and NLRGs. Outside the opaque torus is a region that has slower moving clouds of gas and is called the "narrow-line region". This region produces narrow emission lines because there is less Doppler broadening. These different regions can be seen in Figure 1.1.

When the accretion rate is lower than 0.01 of the Eddington limit, and the accretion flow is geometrically thick, the radiation from the accretion flow is insignificant. However, interactions between the BH and the accretion flow can produce an energetic outflow of charged particles in the form of collimated jets along the poles of the disk that emit strongly at radio wavelengths. This interaction depends on the BH's characteristics, such as its mass and spin, and the structure of the accretion flow (which is mainly determined by the accretion rate of matter onto the BH). These jets can affect the continuum emission of the AGN through synchrotron and inverse Compton processes at all wavelengths from radio waves to gamma rays. However, the most obvious observational effects are at radio wavelengths. Outflows of jets can form giant radio sources or "lobes" that emit synchrotron radiation[2]. Figure 1.2 shows a VLA radio image of Cygnus A taken from Perley et al. (1984). Two radio lobes can be seen, as well as a jet on the right side extending from the galaxy to a giant lobe. The presence of jets and lobes can explain most of the differences between radio loud and radio quiet AGN.

Therefore, although various classes of AGN show different observational features, the above picture suggests a "unified" model which is able to explain all of the various

[2]Synchrotron radiation is an electromagnetic radiation emitted by high-energy particles when accelerated to relativistic speeds in a magnetic field.

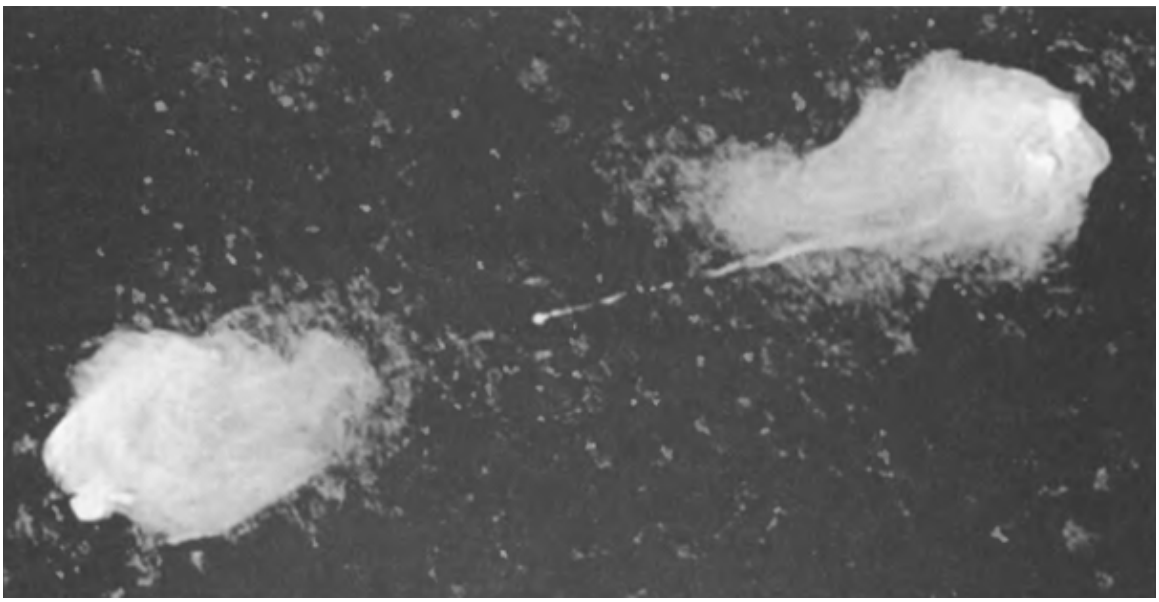

Figure 1.2 A VLA radio image of Cygnus A. Two radio lobes and the jet on the right side extending from the galaxy to a giant lobe can be seen. The separation of the two lobes is around 140 kpc.

types. This unified model is based on an accretion disk orbiting a massive black hole. Different orientations, the presence of a torus, and varying mass accretion rates and BH characteristics can result in different features that determine the type of the observed AGN (see Figure 1.1). While many of the details of this scenario are still uncertain, the unified model is successful in explaining the general features of AGNs, and can lead to a deeper understanding of active galaxies.

1.3 AGN, Jets and Radio Lobes

Although various observed features can be used to classify AGN types, an obvious basic categorization of AGN is whether they are radio loud or radio quiet. Radio loudness is caused by a radio core, one or two jets, and two dominant radio lobes. While the exact physical mechanism behind the radio emission is unclear, there are some models that suggest how this configuration forms in a galaxy. Jets of charged particles are ejected at relativistic speeds from the central nucleus of the AGNs. The outflow in the form of a jet has a high kinetic energy and travels outward into both the interstellar medium of the host galaxy and the intergalactic medium beyond it. The jet faces resistance from the ambient material leading to the deceleration of the jet and the formation of a shock front. As more material is carried outward by the jet, large lobes can form (Figure 1.2). These lobes contain enormous amounts of energy in the form of the kinetic energy of the charged particles and the energy of the magnetic field within the lobes. They can emit synchrotron radiation, and are obvious in radio images. The existence of these large lobes is also confirmed with X-ray images — the formation of the lobes pushes the ambient material in the halo away which creates regions with a deficit in X-ray emission compared to the hot plasma normally found in the halo. These X-ray deficient regions are called “cavities”. The superposition of radio and X-ray images confirms that radio lobes and X-ray cavities are associated with identical regions and probably have the same origin. In addition to the stored energy in the lobes, the formation and expansion of these lobes/cavities can do a considerable amount of work on the ambient material. This implies that the central BH should inject a significant amount of energy into the host galaxy, which emphasizes the importance and role of a super massive BH in the center of active galaxies.

The jets in the AGNs are usually highly collimated structures, and are also known as Poynting-flux dominated jets since the energy and angular momentum from the ac-

cretion flow are carried mainly by the electromagnetic field (Benson & Babul, 2009). The material in the accretion flow is ionized and highly conductive and therefore produces a magnetic field as it orbits the BH. When a whirling BH is present, the rotation of the BH causes a time variation of the magnetic fields attached to the BH, which induces an electric field. A Poynting vector defined by these magnetic and electric fields can represent the directional energy flux density in the jets. Thus, altogether, the magnetized, rapidly rotating accretion flow, with the help of the rotation of the BH, can produce the highly collimated, Poynting-flux dominated jets during the AGN activities.

The presence of magnetic fields, and the interaction between the BH and the accretion flow because of these fields, can cause torques on the whirling BH that on the one hand, can partially power the jet[3], and on the other hand, can limit the spin[4] (Thorne, 1974; Krolik, 1999; Gammie, 1999; Li, 2000, 2002; Agol & Krolik, 2000). It also has been shown that as the spin increases, the kinetic energy of a whirling BH plays a more important role in the jet formation; not only can a more powerful jet form with a higher BH spin, but also a larger fraction of the jet's energy is extracted from the rotating BH rather than the energy of the accretion flow (Benson & Babul, 2009).

Whatever the source of the energy is, the BH must be fed in some way in order to be able to produce a jet. There are different sources of material available to be accreted, such as stars, hot gas from the halo, or cold gas. Stellar accretion is inefficient due to its long accretion timescale, as has been shown by Wang & Hu (2005). Although the timescale for stellar accretion might decrease in an environment of high stellar density and in the presence of an accretion disk (Miralda-Escudé & Kollmeier, 2005), low stellar density of central regions in systems such as brightest cluster galaxies (BCGs) increase the timescale to much longer than the age of the universe.

Hot gas in the galactic halo can also be accreted by a BH. The mechanism which is usually invoked for hot gas accretion is the Bondi accretion model (Bondi, 1952). This model assumes a spherically symmetric flow with negligible angular momentum onto a non-luminous central source. The rate of accretion is called the Bondi accretion rate and can be written as $\dot{M}_{Bondi} = \pi\lambda c_s \rho r_b^2$ where $r_B = 2GM_{BH}/c_s^2$ is the accretion

[3]Blandford & Znajek (1977) were who first suggested a mechanism which makes it possible to extract rotational energy from the black hole.

[4]Note that mass accretion can increase the spin of the BH since the BH can gain angular momentum from the accreted mass (Bardeen, 1970).

radius, G is the gravitational constant, M_{BH} is the black hole mass, c_s is the sound speed of the gas at r_B, ρ is the density of the gas at r_B, and λ is a numerical coefficient that depends on the adiabatic index of the gas. It has been shown that enough hot gas is available in some systems to produce the observed jet power via Bondi accretion (Di Matteo et al., 2000; Allen et al., 2006; Rafferty et al., 2006).

The other potential source of accretion is cold gas from the cooling flow of the intracluster medium (ICM) in the center of the galaxy cluster. The ICM at the centers of many galaxy clusters is so dense that it can cool rapidly (e.g. Lea et al., 1973; Cowie & Binney, 1977; Mathews & Bregman, 1978) and form cool core clusters. This cooling process forms a flow toward the central regions which is known as cooling flow. This cooling flow can provide an important reservoir of cold molecular gas that can be consumed later by both BH accretion and star formation.

Besides the fuel available for accretion onto the BH, jet formation also depends on the structure of the accretion flow that transports the accreted material. It has been shown that when accretion proceeds via a geometrically thick advection-dominated accretion flow (ADAF), jet formation is most efficient (Meier, 2001; Churazov et al., 2005), while it is least efficient in a geometrically thin accretion disk (Livio et al., 1999; Meier, 2001; Maccarone et al., 2003). In an accretion flow, viscosity causes the material to lose angular momentum, which also heats up the material. In a thin disk, materials lose this dissipative energy via radiation (Shakura & Sunyaev, 1973). Since radiation is not efficient when the density is too low, the accretion rate (which represents the density) needs to be higher than the critical value of 0.01 of the Eddington limit, to stay in the thin disk mode. For an accreting BH with an assumed mass to energy conversion of 0.1, the Eddington accretion rate is $22 M_{BH}/10^9$ $\mathrm{M_\odot yr^{-1}}$. However, efficient cooling is not a proper assumption for accretion rates lower than 0.01 of the Eddington accretion rate. Narayan & Yi (1994) suggested that dissipative energy from viscosity can be stored in the entropy of the material in the flow instead of being radiated when radiation is inefficient. This inefficiency in radiation can heat up the disk, and eventually puff the disk up into a torus of hot ions that support the pressure. This geometrically thick flow is favourable for the magnetohydrodynamic (MHD) interactions between a BH and an accretion flow that lead to the formation of a jet.

While the details of the exact mechanisms of jet formation are not yet clear, combining the results from simulations with various analytical models provides a useful framework to study AGNs. Moreover, comparing the results of these models

with observations can put strong constraints on uncertain parameters or assumptions, and can help to better understand the phenomena in active galaxies.

1.4 AGN and MS0735

Active galactic nuclei (AGNs) are a common feature in the central galaxies of cool core clusters (McNamara et al., 2000; Blanton et al., 2001). Typically, there are two modes of AGN activities: quasar or thin disk accretion mode, and radio or advection-dominated accretion flow (ADAF) mode. Observations show clear evidences for a significant amount of star formation (SF) associated with the quasar mode, while it has been shown that this is not the case during the ADAF mode (e.g. Tadhunter et al., 2007). In other words, the amount of SF can vary over a large range, and there is not always a considerable amount of SF accompanying the radio mode.

AGN activities, in the form of jets and X-ray cavities (or the radio mode), are believed to be the reason why the observed cooling flows are generally weaker than predicted (e.g. David et al., 2001; Johnstone et al., 2002; Peterson et al., 2003, and references therein). AGN feedback has been invoked as a way to solve long standing problems such as the overproduction of stars in massive galaxies, or the inability of models to reproduce the colour bimodality in galaxy colour-magnitude diagrams (Baldry et al., 2004). While the effect of radio mode feedback on the intracluster medium (ICM) is generally accepted, it is widely *assumed* that quasar mode feedback can also heat up the ICM and affect SF. However, this is a largely untested assumption. Whether quasar mode radiation can be coupled to the ICM efficiently and provide strong feedback is a matter of debate. Considering the above point, cases with a high amount of SF during the quasar mode and a low amount of SF during the radio (ADAF) mode are not surprising.

The observed empirical relations between black hole mass and bulge properties such as luminosity or mass (Kormendy & Richstone, 1995; Magorrian et al., 1998; Ferrarese & Merritt, 2000; Gebhardt et al., 2000; Marconi & Hunt, 2003; Häring & Rix, 2004) are commonly cited as evidence of the coupling between star formation and BH mass growth. One of the most common forms of these observed relations is the scaling relation between BH mass (M_{BH}) and bulge stellar mass (M_{bulge}) in the local universe, known as the Magorrian relation (Magorrian et al., 1998). This observed relationship has been interpreted as a co-evolution of M_{BH} and M_{bulge} which requires a feedback mechanism to couple the M_{BH} and bulge properties. If one assumes that

the majority of the change in the BH mass is due to quasar mode accretion, and that this mode is accompanied by coupled SF, then the Magorrian relation implies a ratio of change in M_{bulge} to M_{BH} ($\Delta M_{bulge}/\Delta M_{BH}$) or, identically, a ratio of average star formation rate (SFR) to average BH accretion rate (BHAR), of around a few hundred (e.g. Magorrian et al., 1998; Marconi & Hunt, 2003) during the quasar mode.

Here, we seek to situate the AGN outburst observed in the galaxy cluster MS0735.6+7421 (Figure 1.3) within the context of this general understanding.

1.4.1 Observation

The energy of a typical AGN burst is around 10^{58} erg (Bîrzan et al., 2004; Rafferty et al., 2006), but systems such as MS0735.6+7421, Hercules A, Hydra A, and 3C 444 have outburst energies of $\geq 10^{61}$ erg (McNamara et al., 2005; Nulsen et al., 2005; Wise et al., 2007; Croston et al., 2011). The most energetic AGN outburst so far has been observed in the galaxy cluster MS0735.6+7421, with a total energy of around 1.21×10^{62} erg (McNamara et al., 2009). The age of the burst has been estimated to be 1.1×10^{8} yr, assuming a spherical model for the shock produced by cavities (McNamara et al., 2005), which suggests a lower limit for the mean power of 3.5×10^{46} erg s^{-1}, assuming the jets were on for the whole 1.1×10^{8} yr.

McNamara et al. (2009) used the XMM-Newton Optical Monitor Wide 1 (W1 - 291 nm) UV image to estimate the star formation rate in MS0735. They found a UV luminosity of 1.82×10^{42} erg s^{-1} within a 10" aperture (MS0735 is at redshift $z = 0.216$ where 1" corresponds to 3.5 kpc). They estimated a current star formation rate of 0.25 $M_{\odot}yr^{-1}$ using the relation given by Salim et al. (2007). While the typical star formation rate in the central galaxies in cool core clusters is found to be $\sim 0.5 - 10$ $M_{\odot}$ yr^{-1} (up to the order of 100 $M_{\odot}$ yr^{-1} for extreme cases - Hicks & Mushotzky, 2005; McNamara et al., 2006; Bildfell et al., 2008; Pipino et al., 2009, and references therein), a fairly low SFR of 0.25 $M_{\odot}yr^{-1}$ in this system is not surprising since it has recently experienced a very energetic radio mode AGN outburst. However, explaining this very energetic AGN outburst is found to be challenging (McNamara et al., 2009).

1.4.2 MS0735 and Challenges

Generally, it is believed that gas accretion onto a super massive black hole is the engine powering AGNs. The jet energy output (E_{jet}) of an AGN depends on the

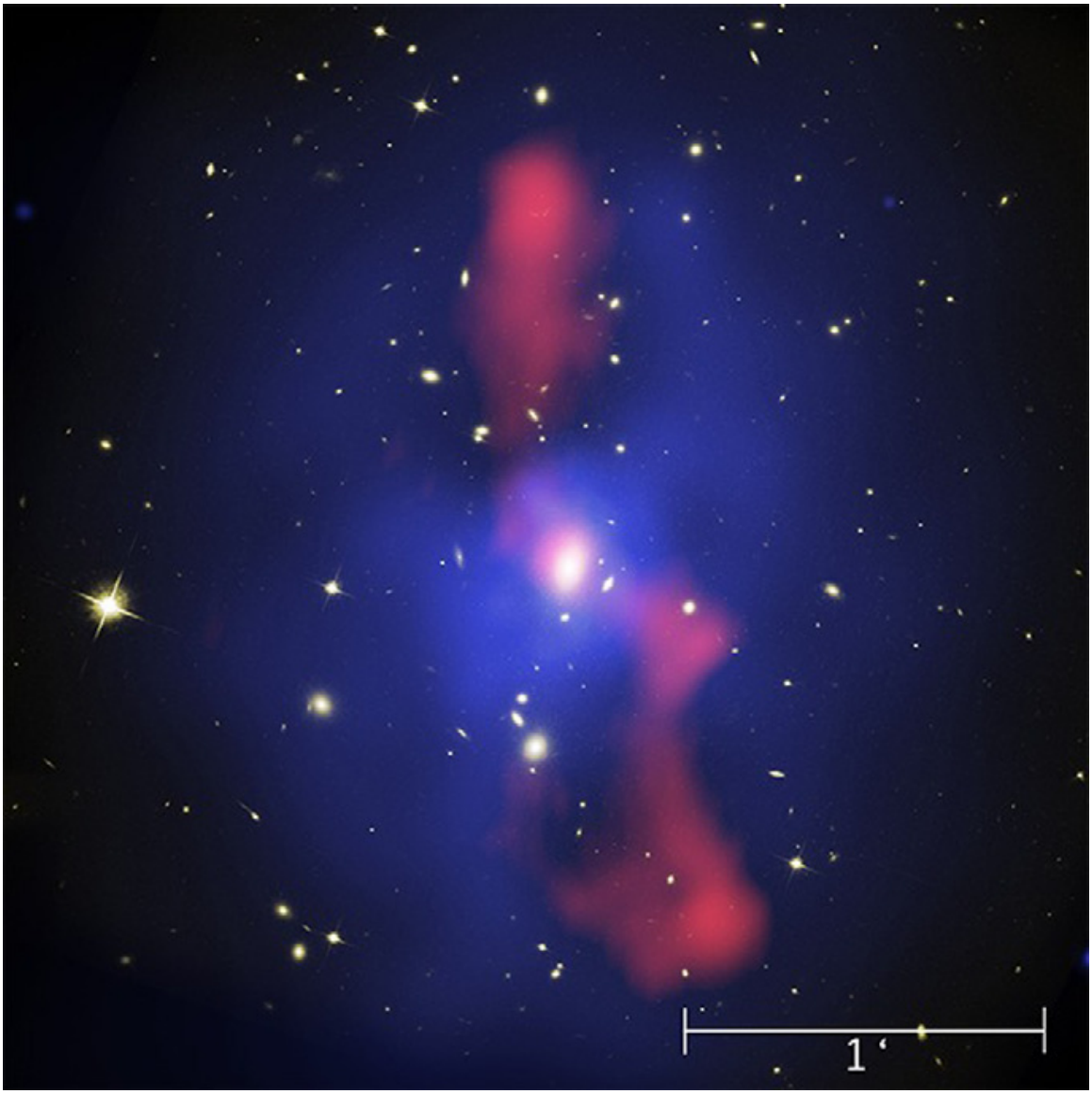

Figure 1.3 A combined image of MS0735+7421 cluster. Blue, white and red colours correspond to X-ray, I-band and radio wavelengths, respectively (McNamara et al., 2009).

mass accreted onto the BH (ΔM_{acc}) and a mass to energy conversion efficiency (ϵ). For a constant ϵ, one can write:

$$E_{jet} = \epsilon \Delta M_{acc} c^2 \tag{1.1}$$

or identically:

$$E_{jet} = \frac{\epsilon}{(1-\epsilon)} \Delta M_{BH} c^2 \tag{1.2}$$

where ΔM_{BH} is the change in M_{BH} and c is the speed of light. Similarly, the power output (P_{jet}) depends on the rate of rest mass accretion ($\dot{M}_{acc}$), the rate of change in M_{BH} ($\dot{M}_{BH}$) and ϵ as follows:

$$P_{jet} = \epsilon \dot{M}_{acc} c^2 \tag{1.3}$$

$$P_{jet} = \frac{\epsilon}{(1-\epsilon)} \dot{M}_{BH} c^2. \tag{1.4}$$

If one assumes a typical value of $\epsilon \sim 0.1$, for a system like MS0735 with $E \sim 1.21 \times 10^{62}$ erg and $P_{jet} \geqslant 3.5 \times 10^{46}$ erg s^{-1}, the required ΔM_{acc} and $\dot{M}_{acc}$ are $\sim 6.7 \times 10^8$ M$_\odot$ and $\geqslant 6.1$ M$_\odot$ yr^{-1}, respectively. However, the radio mode is associated with low gas accretion rates onto the BH, and the required gas accretion rate in order to explain the outburst is higher than what is generally accepted for the radio mode.

As was discussed in the previous sections, jets can form when accretion happens via an ADAF (Narayan & Yi, 1995), but the structure of the accretion flow itself depends on the accretion rate. Accretion via an ADAF happens when the accretion rate is lower than the critical rate of 0.01 of the Eddington accretion rate (Narayan & Yi, 1995). This constraint puts an upper limit on possible accretion rates and the total accreted mass during the ADAF mode for a given M_{BH}. For a $M_{BH} \sim 5 \times 10^9$ M$_\odot$ (as has been suggested for MS0735; McNamara et al. 2009), 0.01 of the Eddington accretion rate corresponds to 1.1 M$_\odot$ yr^{-1} which is much lower than the minimum mean rate of 6.1 M$_\odot$ yr^{-1} required to explain the AGN outburst. Thus, the required mass and accretion rate for the AGN outburst in this system cannot be explained with the above constraints.

McNamara et al. (2009) have grappled with this problem and proposed two possible solutions: either the BH must be much more massive (to have a higher Eddington accretion rate; McNamara et al. 2009), or ϵ should be higher so that a lower amount of accreted mass can produce the same amount of the energy (McNamara et al., 2011). An ultra-massive BH (with mass $> 10^{10}$ M$_\odot$) in a system like MS0735 is not

consistent with what is generally believed from observations (e.g. Marconi & Hunt, 2003). To avoid an ultra-massive BH in this system, ϵ must be increased. However, the efficiency of the mass to energy conversion depends on the BH's spin (Benson & Babul, 2009); higher ϵ can be achieved with a higher spinning BH. Here, we explore the second solution in detail, and ask the question: How could the BH spin up to very high spins in advance of the outburst? Very high spin states are unstable; BH will spin down rapidly and tend to the equilibrium spin (Benson & Babul, 2009) where $\epsilon \sim 0.1$. We also explore the attendant physical processes, such as SF, during the spin-up mode and investigate the associated observational implications.

A ΛCDM cosmology with a Hubble constant of $H_0 = 70$ kms^{-1}Mpc^{-1} and a mass density parameter of $\Omega_m = 0.3$ has been assumed through this work. The redshift of MS0735 is $z = 0.216$.

Chapter 2

Spinning up the BH

2.1 The Basic Scenario for Spinning up the BH

There are two ways to increase the BH spin: one is via gas accretion, and the other is via a merger with another BH. We explore these mechanisms to spin up the BH and investigate possible solutions that can explain the AGN outburst in the MS0735. For the sake of simplicity, we define our basic scenario for spinning up the BH as a pure gas accretion scenario, and we will later investigate whether considering a BH-BH merger can change our results or conclusion.

We consider a long-term scenario to explain the burst in MS0735. We assume that first the BH has experienced a gas accretion period via a thin disk (or a quasar mode) that spins it up. No jet can form during this mode and the BH can be spun up efficiently (Benson & Babul, 2009). When the spin becomes high enough, we assume that the accretion mode switches to an ADAF and jet formation becomes possible.

Under the above scenario, jet formation is not triggered until the BH spin is high enough to satisfy the constraints on the accretion modes. The main constraint is to keep the accretion rate lower (or higher) than the critical rate of 0.01 of the Eddington accretion rate for the ADAF (or thin disk) mode. We also assume the time duration of the ADAF to be $\sim 1.1 \times 10^8$ yr which implies a lower limit of power output.

We now define the starting point of our scenario. It has been shown that the BH spin distribution depends on the amount of material accreted in a single accretion episode (Volonteri et al., 2007; King et al., 2008; Fanidakis et al., 2011). If the mass accreted during each event fragments into multiple, randomly aligned accretion episodes with masses much lower than M_{BH}, then the average spin of the final

distribution becomes very low (e.g. King et al., 2008). However, the final spin distribution skews toward higher values if accretion happens via a single accretion episode (or multiple aligned accretion episodes) with a comparable mass to M_{BH} (Volonteri et al., 2007). In the latter case, the distribution skews toward the equilibrium spin attained by accreting BHs (Volonteri et al., 2007) which has been suggested to be $j \sim 0.9$, where j is dimensionless spin parameter, by recent magnetohydrodynamic (MHD) simulations (e.g. Gammie et al., 2004). So, while one could start with a non- or slow-rotating BH, we choose a rather high but acceptable value for the initial spin of equilibrium spin of around 0.92 (Benson & Babul, 2009). The choice of a high initial spin helps our scenario by reducing the required amount of accreted mass. Any correction to a lower initial spin results in a higher required amount of accreted mass.

We summarize our scenario as followed. The BH is initially at the equilibrium spin. It starts to accrete via a thin disk (quasar mode) and increases its spin. When the spin becomes high enough, the thin disk switches to ADAF and jet formation becomes possible for a duration of $\sim 1.1 \times 10^8$ yr. We present the results of our calculations in the next chapter.

Chapter 3

Results

First we define the different parameters and explain how we have done our calculations. As stated in the previous section, we consider j to be the dimensionless spin parameter which is defined as:

$$j = Jc/(\mathrm{G}M_{BH}^2) \tag{3.1}$$

where J is the angular momentum of a Kerr black hole of mass M_{BH}, c is the speed of light, and G is the gravitational constant. We consider j_i and j_f to be the initial and final BH spin, respectively. We also define the spin at the beginning of the ADAF mode to be the switch spin, j_s. Moreover, the change in M_{BH} during the thin disk mode and ADAF are $\Delta M_{BH,thin}$ and $\Delta M_{BH,ADAF}$, respectively. The total change in M_{BH} is defined as $\Delta M_{BH,tot} = \Delta M_{BH,thin} + \Delta M_{BH,ADAF}$. Furthermore, we consider $M_{BH,i}$ and $M_{BH,f}$ to be the initial and final BH masses respectively, so that $M_{BH,f} = M_{BH,i} + \Delta M_{BH,tot}$.

We use the model by Benson & Babul (2009) for our BH spin-up calculations. In order to calculate the change in the spin and BH mass, we use their dimensionless spin-up function $s(j)$, which is defined as:

$$s(j) = \frac{dj}{dt}\frac{M_{BH}}{\dot{M}_{acc}} \tag{3.2}$$

or identically,

$$s(j) = \frac{dj}{dt}\frac{M_{BH}}{(1-\epsilon(j))\dot{M}_{BH}} \tag{3.3}$$

where $\dot{M}_{acc}$ and $\dot{M}_{BH}$ are the rate of rest mass accretion and rate of change in M_{BH},

respectively. The parameter $\epsilon(j)$ is the mass-energy conversion efficiency, which is a function of j itself. Note that $\epsilon(j)$ is dominated by the radiation and jet efficiency during the thin disk and ADAF mode, respectively. In other words, during the thin mode $\epsilon(j)$ corresponds to the part of the accreted mass which is lost mainly due to radiation, while it corresponds to jet efficiency during ADAF mode.

Considering $dM_{BH} = \dot{M}_{BH}dt$, we can rewrite equation 3.3 as follows:

$$\frac{dM_{BH}}{M_{BH}} = \frac{s(j)}{1-\epsilon(j)}dj. \tag{3.4}$$

One can find the required change in BH mass needed to change the spin from one value to another using equation 3.4. We calculate $\Delta M_{BH,thin}$ for different choices of $M_{BH,f}$ and j_s using the corresponding $s(j)$ and $\epsilon(j)$ provided by Benson & Babul (2009). We investigate all cases which can produce enough energy and satisfy the constraint on the accretion rate, but we only present the results for cases that are "the most efficient". The most efficient case for a given $M_{BH,f}$ is the one that not only can explain the AGN burst and satisfy the various constraints, but also corresponds to the smallest $\Delta M_{BH,thin}$ for that given $M_{BH,f}$. Note that we present the change in BH mass rather than the accreted mass since our final goal is to investigate what our calculations imply about $M_{BH} - M_{bulge}$ scaling relation.

3.1 Results for the Required Change in the Black Hole Mass and Spin

Figure 3.1 shows the corresponding j_s for different $M_{BH,f}$ for the most efficient cases. One can see that less massive BHs must be spun up to higher spins before the ADAF begins in order to produce the same amount of energy. The reason is that the maximum mass that can be accreted during the ADAF is limited by the maximum possible accretion rate of 0.01 of the Eddington accretion rate. However, the Eddington accretion rate is correlated with the BH mass. Therefore, the maximum mass that can be accreted during the ADAF decreases with decreasing BH mass. As a result, less massive BHs should have a higher average ϵ during ADAF, and therefore a higher j_s, in order to produce the same amount of energy.

The lowest $M_{BH,f}$ which can produce a sufficiently energetic burst for our target is around 8×10^8 $M_\odot$. Even a maximally rotating BH with lower mass cannot produce

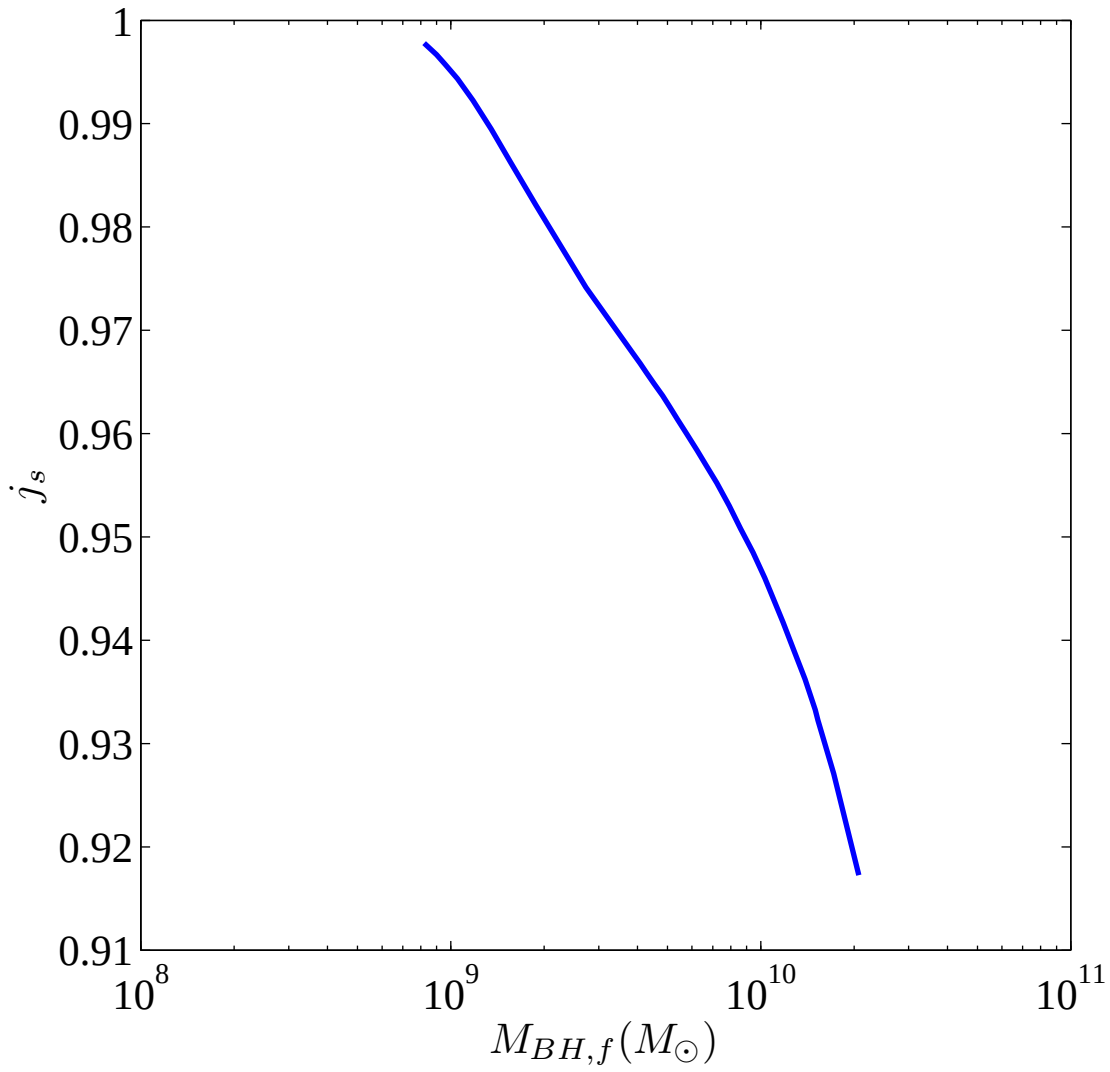

Figure 3.1 Switch spin (j_s) vs. final BH mass for the most efficient cases. The switch spin is the spin at the beginning of the ADAF mode. This figure clearly shows that lower mass BHs must be spun up to higher values in order to fit within our scenario.

enough energy since it cannot accrete enough mass during the ADAF mode. Note that the maximum spin that can be achieved via thin disk accretion is limited to $j \sim 0.998$ since the BH would preferentially swallow negative angular momentum photons emitted by the accretion flow (Thorne, 1974; Benson & Babul, 2009). On the other hand, all BHs with $M_{BH,f} \geq 8{\times}10^8$ $M_\odot$ can potentially produce the burst, so the higher choice of $M_{BH,f}$ for plotting is arbitrary. We choose $M_{BH,f} \sim 2.1 \times 10^{10}$ $M_\odot$ because this is the first M_{BH} which is able to produce enough power and energy and satisfy our constraints without needing to be spun up. In other words, BHs with $M_{BH,f} \geq 2.1 \times 10^{10}$ $M_\odot$ can stay at equilibrium spin during ADAF, with an efficiency of ~ 0.13, and form sufficiently powerful jets. Thus, for all cases with $M_{BH,f} \geq 2.1{\times}10^{10}$ $M_\odot$, j_s is the same and is equal to the equilibrium spin. Therefore, we do not plot j_s for $M_{BH,f} > 2.1 \times 10^{10}$ $M_\odot$.

Figure 3.2 displays the corresponding fraction of change in BH mass during thin disk accretion, $\Delta M_{BH,thin}/M_{BH,f}$, for the most efficient cases of different $M_{BH,f}$. It clearly shows that less massive BHs should accrete a higher ratio of their mass since they need a higher j_s.

Discussing results in terms of the fraction of change in BH mass is insightful, but since our final goal is to investigate what our results imply about $M_{BH} - M_{bulge}$ scaling relation, we display the real amount of change in BH mass during the thin disk mode ($\Delta M_{BH,thin}$) in Figure 3.3. Once again, it shows that $\Delta M_{BH,thin}$ is zero for $M_{BH,f} \geq 2.1 \times 10^{10}$ $M_\odot$ which means there is no need to spin up BHs with $M_{BH,f} \geq 2.1 \times 10^{10}$ $M_\odot$. Neglecting these cases with ultra-massive BHs, this plot suggests that a change in M_{BH} of a few times 10^8 $M_\odot$ is required during the thin disk (quasar) mode to spin up the BHs to the desired j_s which can produce a sufficiently energetic AGN outburst during ADAF mode.

For the sake of completeness, we also present the corresponding $\Delta M_{BH,tot}/M_{BH,f}$ and $\Delta M_{BH,tot}$ for the most efficient cases. Figure 3.4 shows the corresponding total fraction of change in BH mass ($\Delta M_{BH,tot}/M_{BH,f}$) for the most efficient cases of different $M_{BH,f}$. Note that $\Delta M_{BH,tot}/M_{BH,f}$ is smaller than $\Delta M_{BH,thin}/M_{BH,f}$ for less massive BHs. This is because ϵ is higher than 1 for very high spin values, and $\Delta M_{BH,ADAF}$ becomes negative. Indeed, efficiencies higher than 1 are possible at the expense of BH rotational energy which results in a decrease in total BH mass.

We also display the real amount of total change in BH mass ($\Delta M_{BH,tot}$) in Figure 3.5. Once again, $\Delta M_{BH,tot} = \Delta M_{BH,thin} + \Delta M_{BH,ADAF}$. This figure shows that while $\Delta M_{BH,tot}/M_{BH,f}$ is higher for less massive BHs, $\Delta M_{BH,tot}$ is lower for these cases

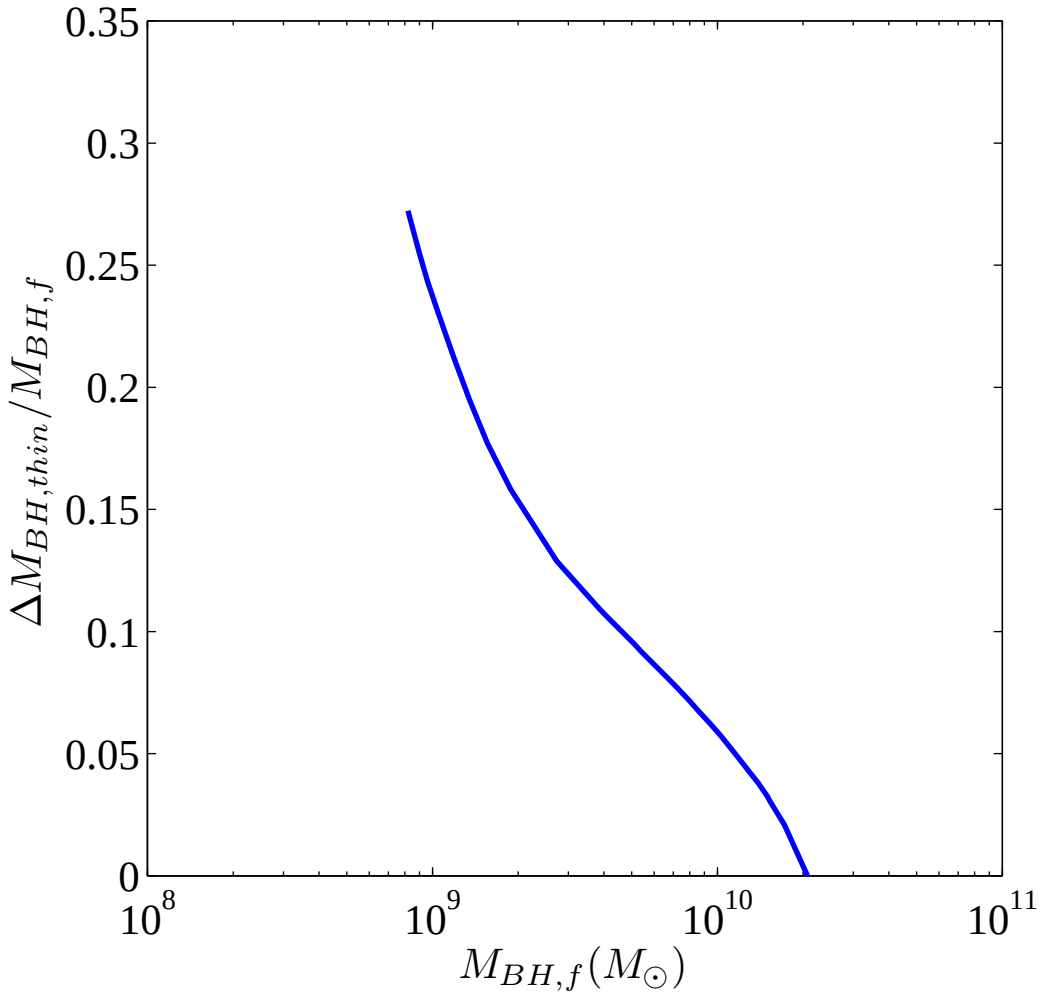

Figure 3.2 The fraction of change in final BH mass during thin mode vs. BH mass for the most efficient cases. Lower mass BHs have to accrete a higher fraction of their mass since they have to get to higher j_s.

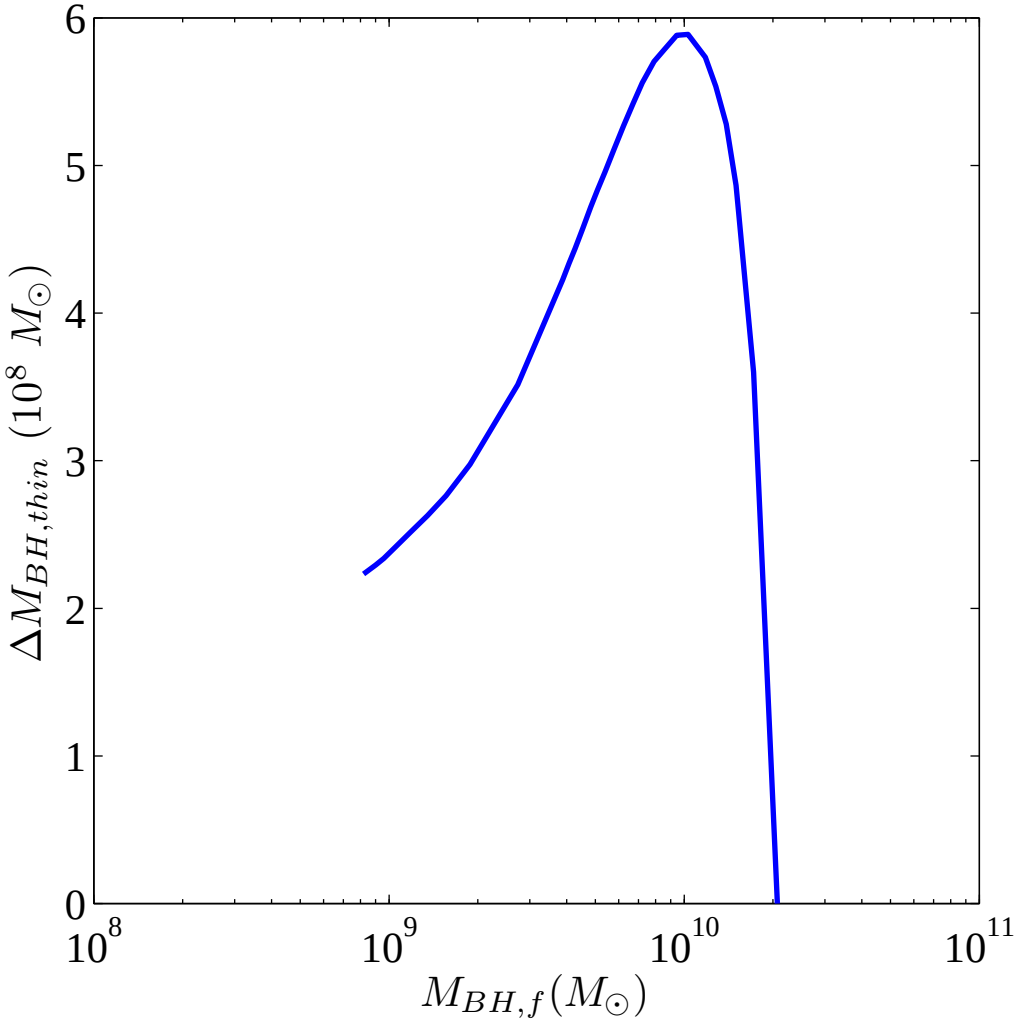

Figure 3.3 The real amount of change in BH mass during thin disk mode (in solar mass) vs. final BH mass for the most efficient cases.

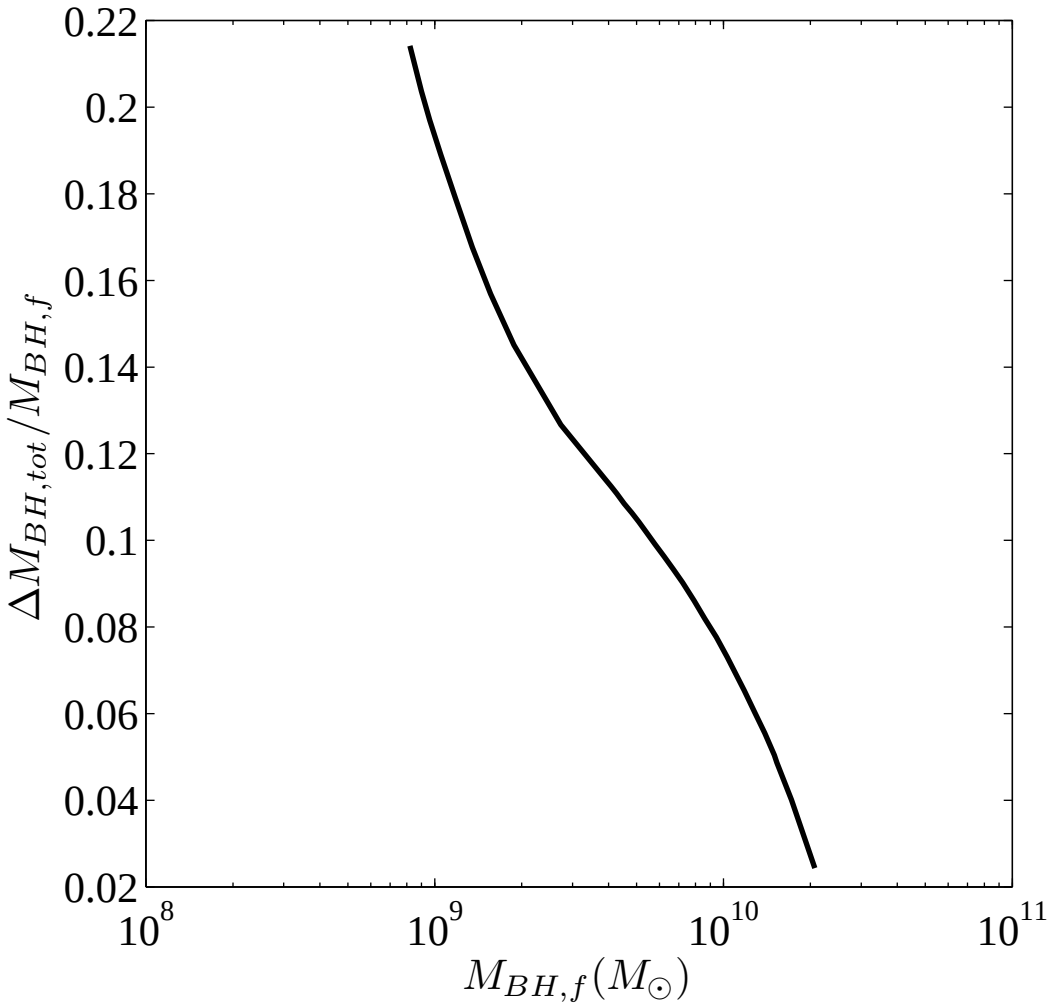

Figure 3.4 The total fraction of change in final BH mass vs. BH mass for the most efficient cases.

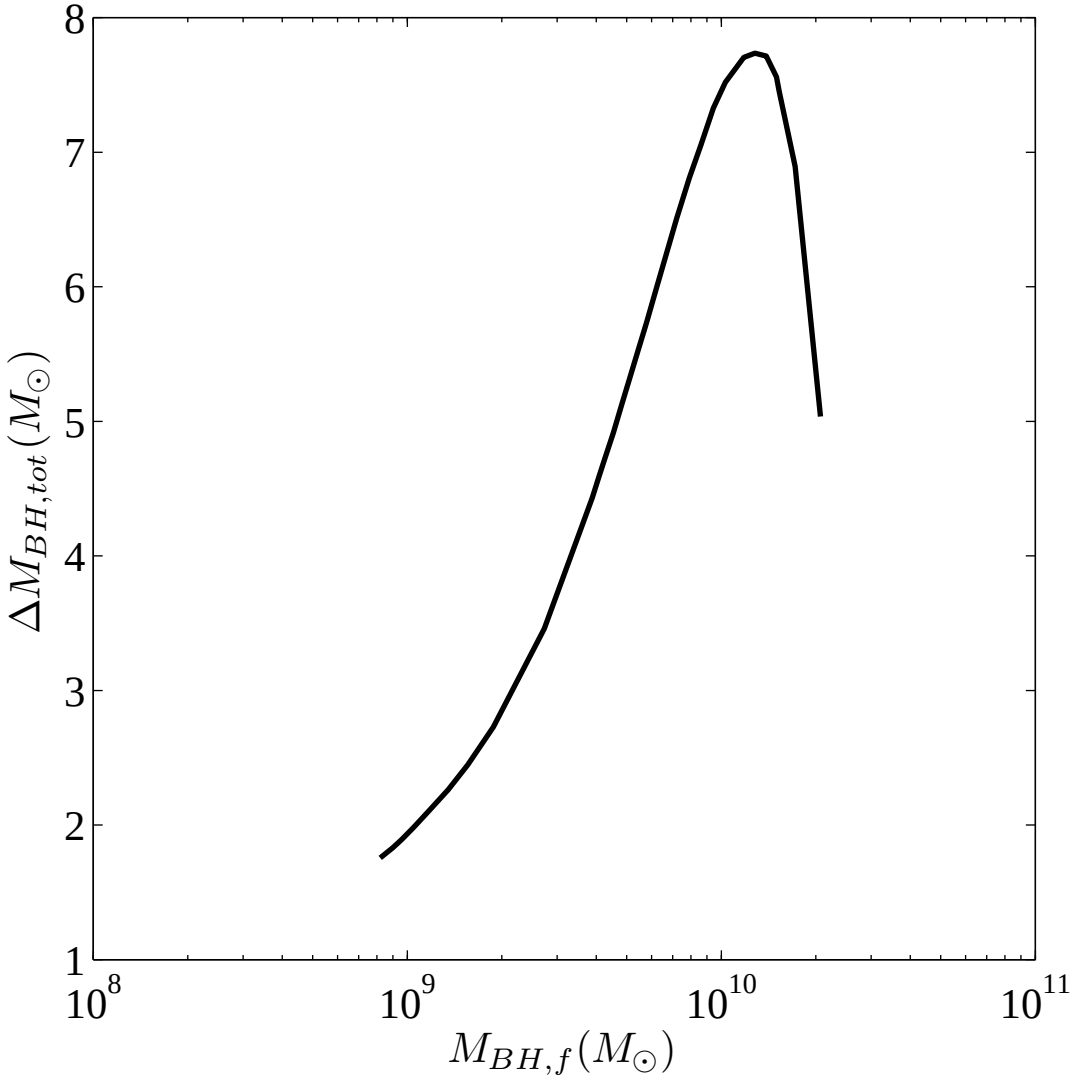

Figure 3.5 The real amount of change in BH mass (in solar mass) vs. final BH mass for the most efficient cases. The lowest change corresponds to the lowest BH mass.

compared to more massive BHs. Also, although $\Delta M_{BH,tot}$ decreases after some point, it does not continue for $M_{BH,f} \geq 2.1 \times 10^{10}$ $M_\odot$. As was discussed above, the most efficient cases for $M_{BH,f} \geq 2.1 \times 10^{10}$ $M_\odot$ are cases that remain at equilibrium spin. Since all these cases have the same constant efficiency, $\Delta M_{BH,ADAF}$ is the same for all of them, and the decrease in $\Delta M_{BH,f}$ does not continue after $M_{BH,f} \sim 2.1 \times 10^{10}$ $M_\odot$.

In the next section, we present the results of the spinning up scenario that includes a BH-BH merger.

3.2 BH-BH Merger

In this section, we investigate whether considering a BH-BH merger scenario to spin up the BH can change our results as compared to a pure gas accretion scenario. For the purpose of comparison with our basic scenario, we consider the merger of two BHs which are at equilibrium spin. We use the results of Kesden (2008) to calculate the state of the final BH after merger. The corresponding relation for the BH spin after merger (j_{merge}) is as following (Kesden, 2008):

$$j_{merge} = \frac{\nu L_{ISCO}(j_{merge}) + \frac{j_1}{4}(1+\sqrt{1-4\nu})^2 + \frac{j_1}{4}(1+\sqrt{1-4\nu})^2}{\{1-\nu[1-E_{ISCO}(j_{merge})]\}^2}. \qquad (3.5)$$

The quantity ν is the symmetric mass ratio and is defined as $\nu = (M_{BH,1}M_{BH,2})/(M_{BH,1}+M_{BH,2})^2$ where $M_{BH,1}$ and $M_{BH,2}$ are the primary and secondary BH mass, respectively ($M_{BH,1} \geq M_{BH,2}$). The variables j_1 and j_2 are the spin of $M_{BH,1}$ and $M_{BH,2}$ just before the coalescence, and are assumed to be aligned. Also, L_{ISCO} and E_{ISCO} are the (dimensionless) specific angular momentum and specific energy of the innermost stable circular orbit (ISCO) of the BH, respectively (The ISCO is the orbit inside of which the centrifugal force is unable to balance gravity and the gas begins to free-fall inward).

We define q as the mass ratio of the secondary to primary, $q = M_{BH,2}/M_{BH,1}$. We use relation 3.5 to find the required q for a given j_{merge}. Figure 3.6 shows the results for different cases of j_{merge}. Note that our primary and secondary BHs are at equilibrium spin, and Figure 3.6 suggests that the merger of two BHs at equilibrium spin cannot result in spins higher than ~ 0.985.

In the above scenario, the final spin after the merger (j_{merge}) is the spin at the beginning of the ADAF mode. Indeed, it is the same as the switch spin (j_s) in the gas accretion scenario. Therefore, we combine Figure 3.1 and 3.6 to find the corresponding

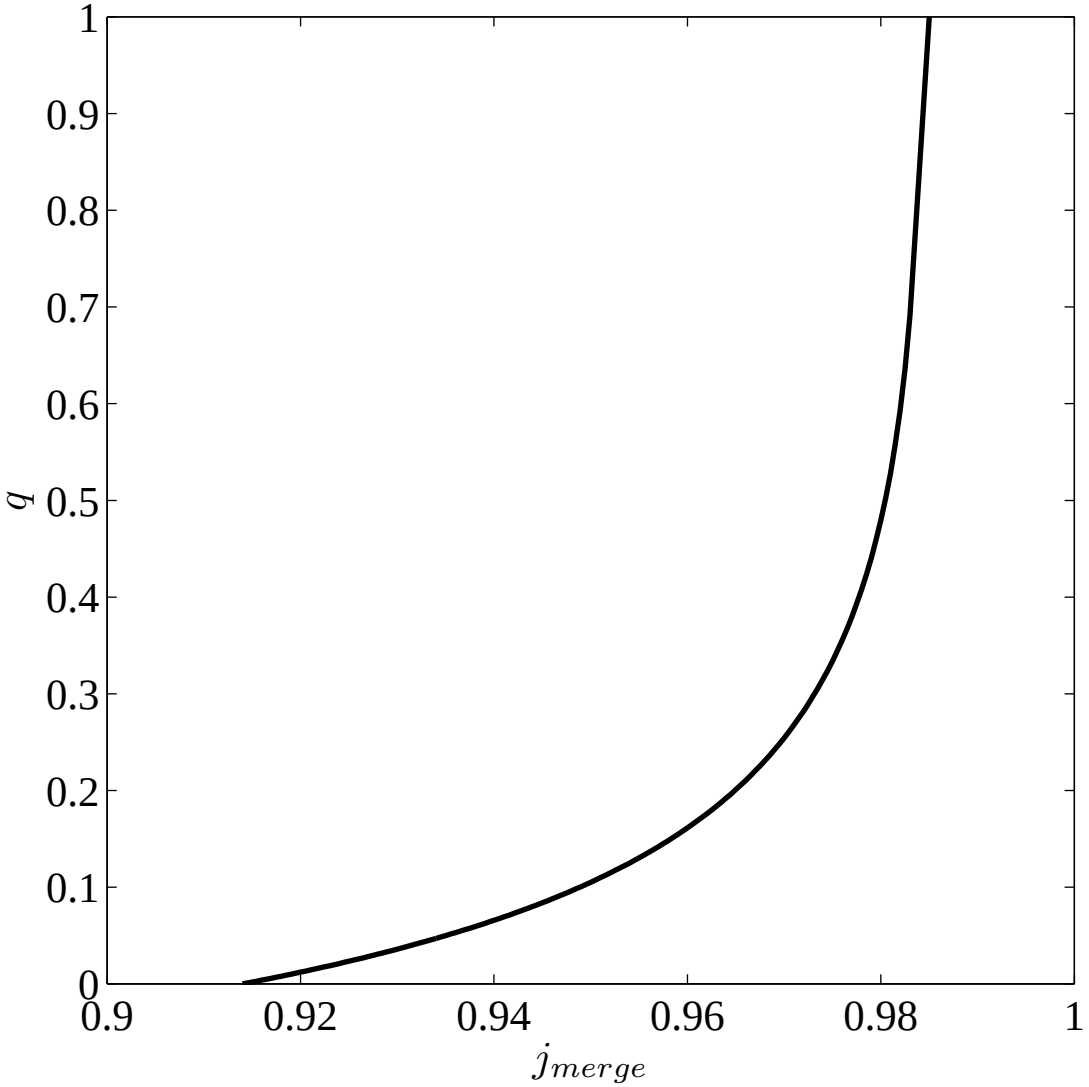

Figure 3.6 The mass ratio of the secondary to primary BH (q) vs. the spin of the BH after the merger (j_{merge}). The BHs are at equilibrium spin before the coalescence. The highest achievable spin is ~ 0.985.

minimum required q for a given $M_{BH,f}$. Figure 3.7 shows the results. The $M_{BH,f}$ that corresponds to $j_s \sim 0.985$ is around 1.7×10^9 $M_\odot$. For larger $M_{BH,f}$, all cases with q above the plotted value in Figure 3.7 can potentially have a sufficiently high j_s to produce a sufficiently energetic AGN burst during the ADAF mode.

One should note that if BHs could be spun up to spins higher than equilibrium before the coalescence, not only could a value of $j_{merge} > 0.985$ be achieved, but a smaller q would also be required for all cases. However, the only scenario to spin up a BH other than a BH-BH merger is gas accretion. The larger the amount of accreted gas, the higher the spin is before the coalescence. Thus, a higher j_{merge} with a smaller q can be achieved with a larger amount of accreted gas. At the limit of $q \to 0$, all the solutions converge to the pure gas accretion scenario. Moreover, while one might assume a *pure* BH-BH merger in order to spin up the BH and consider any solution from the parameter space in Figure 3.7 as an explanation, it should be noted that a *pure* BH-BH merger without any gas accretion cannot be a practical scenario for this system as we discuss in the following paragraphs.

The coalescence of BHs is a long standing problem. Two BHs can be brought to about 1 pc of each other during a merger as a result of the dynamical friction with background stars. Dynamical friction is the loss of momentum and kinetic energy of moving bodies through a gravitational interaction with surrounding matter in space (Chandrasekhar, 1943), but this mechanism is insufficient for creating smaller separations than 1 pc (Begelman et al., 1980; Milosavljević & Merritt, 2001). The ultimate coalescence of the BHs can happen due to efficient gravitational radiation[1] when their separation becomes smaller than 1 pc by a factor of ~ 100 (Milosavljević & Merritt, 2001). However, going from 1 parsec to that smaller separation is a challenge and is known as the "final parsec problem". Different mechanisms can be invoked to explain the final parsec problem but finding a comprehensive solution is not an easy task. While dynamical friction from the stellar background is not efficient at smaller separations than 1 pc, interactions between BHs and a gas disk at small separations has been invoked as a standard solution in order to extract angular momentum from the binary BH, and therefore effect the coalescence (Ivanov et al., 1999; Armitage & Natarajan, 2002; Milosavljević & Phinney, 2005; Dotti et al., 2006; Loeb, 2007; Cuadra et al., 2009).

The issue in the final parsec problem for the merger of SMBHs is the very large

[1]Gravitational radiation is a fluctuation in the curvature of spacetime which propagates as a wave, travels outward from the source, and theoretically can transport energy.

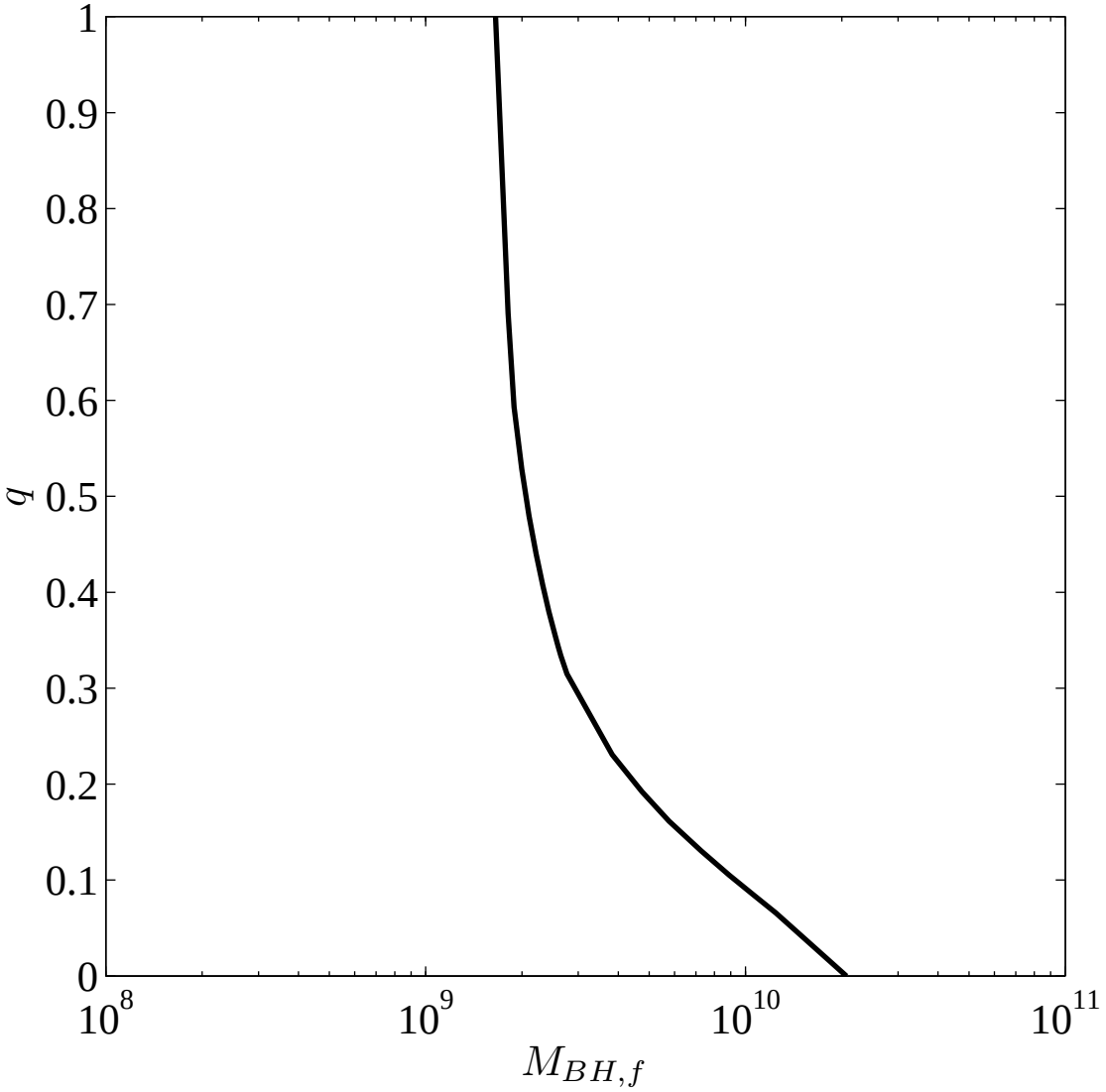

Figure 3.7 The spin of the BH after merger (j_{merge}) vs. final BH mass. This plot combines Figure 3.1 and 3.6. For a given $M_{BH,f}$ all cases with q above the plotted value can potentially have a sufficiently high j_s to produce a sufficiently energetic AGN burst during the ADAF mode.

required timescale (on the order of a Hubble timescale) to go from 1 pc to a separation where gravitational radiation is efficient. A circumbinary gas disk can facilitate the coalescence and decrease the required timescale from a Hubble timescale to an acceptable timescale of less than 1 Gyr (Lodato et al., 2009). However, the circumbinary gas disk is unstable to star formation at around 0.1 pc, and star formation increases the coalescence timescale again to longer than 1 Gyr. Moreover, the coalescence timescale also depends on the total disk mass (e.g. Cuadra et al., 2009). Lodato et al. (2009) found that the disk mass should be at least comparable to the secondary mass to produce the merger (one should note that even for this value, their BHs' initial separation was around $0.01 - 0.05$ pc rather than 1 pc). Thus, a realistic case for a BH-BH merger within a reasonable timescale is not possible without gas accretion.

Moreover, one should also note that studies such as Kesden (2008) assume BHs with aligned spins, whose merger will not produce a kick of several thousand kilometers per second. This is another challenge of BHs mergers, which implies that many galaxies would not have a BH in the central region if merging BHs can not align themselves before the coalescence. However, there are some mechanisms, such as the one discussed by Bogdanović et al. (2007), that help the BHs to align their spin before the coalescence. Bogdanović et al. (2007) suggest that if BHs accrete $1 - 10\%$ of their masses during a merger, torques from accreted gas can align the BHs' spin with the orbital axis and the large-scale gas flow. Considering this, we assumed that the BHs are aligned when they merge, as is required for the Kesden (2008) calculations.

Despite all the constraints, we use the results of Lodato et al. (2009) and compare the minimum required gas mass for a BH-BH merger and the required gas mass from the pure gas accretion scenario to spin up the BH. Figure 3.8 shows the results. The black dashed line and blue solid line correspond to the required gas mass of BH-BH merger and pure gas accretion scenario, respectively. This plot suggests that even more gas should be present for accretion during a BH-BH merger scenario. This requires a mechanism to bring the gas to the center of the galaxy, which again invokes the SF challenge, similar to the quasar mode. Altogether, even a BH-BH merger scenario does not decrease the required amount of gas in the accretion disk around the BH, and our results for required gas mass do not change.

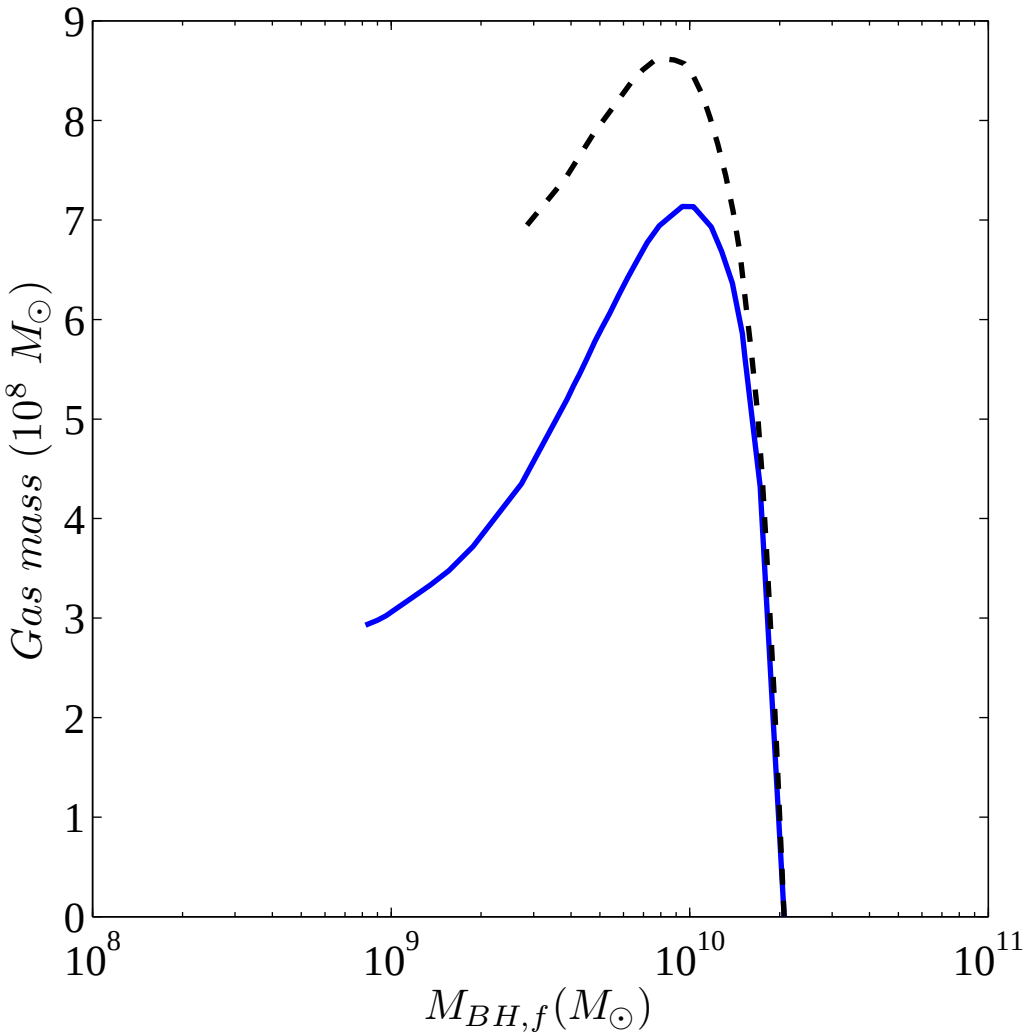

Figure 3.8 The required amount of gas mass for different spinning up scenarios vs. the final BH mass. The black dashed line and blue solid line correspond to the required gas mass of a BH-BH merger and a pure gas accretion scenario, respectively. This plot suggests that even more gas should be present for accretion during a BH-BH merger compared to a pure gas accretion scenario. Note that the blue solid line shows the mass of accreted gas during the quasar mode which is slightly higher than the change in BH mass. This is because part of the accreted gas will be radiated away, and the change in BH mass is slightly lower than the total amount of accreted gas during the quasar mode.

Chapter 4

The Challenge of High SF

As was discussed in the previous sections, jets are typically related to the ADAF mode, and there is evidence that a considerable amount of SF does not always accompany the radio (ADAF) mode (e.g. Tadhunter et al., 2007). Therefore, if one interprets the observed Magorrion relation as a co-evolution of M_{BH} and M_{bulge} with a ratio of a few hundred for $\Delta M_{bulge}/\Delta M_{BH}$, then this interpretation is specific to the quasar mode. In other words, it is usually during a quasar mode that the BH gas accretion is accompanied by a significant amount of star formation. In our proposed scenario to explain the AGN burst in MS0735, the quasar mode corresponds to the BH spin-up phase. Below, we briefly summarize when and why a spin-up phase was required, and how much gas should be accreted during this phase.

Based on our calculations in previous sections, assuming an efficiency of ~ 0.13 (the corresponding efficiency for the equilibrium spin), the required accretion rate during a period of 1.1×10^8 yr of ADAF mode must be ~ 4.6 $M_\odot$ yr^{-1} in order to explain the AGN burst in MS0735. For $M_{BH,f} \geq 2.1 \times 10^{10}$ $M_\odot$, this accretion rate is comfortably below the critical threshold of ~ 0.01 of the Eddington accretion rate and the jet outburst can be attributed to mass accretion via an ADAF. Thus, there is no need for a quasar mode for these cases. However, for the suggested BH mass of 2×10^9 $M_\odot$ or 5×10^9 $M_\odot$ for MS0735 (Rafferty et al., 2006; McNamara et al., 2009), the required accretion rate exceeds the critical threshold of ~ 0.01 of the Eddington accretion rate, and the AGN cannot be in an ADAF mode during the burst. To maintain an ADAF mode during the radio outburst, McNamara et al. (2011) have proposed that the BH must have been spun up to near maximal spins at the start of the outburst. As we have shown in the previous sections, regardless of how one spins up the BH, i.e. via a pure gas accretion or BH-BH merger scenario, the process

requires at least a few times 10^8 $M_\odot$ of gas in an accretion disk around the BH. A BH with an accretion disk is typically in a quasar mode, and based on the discussion in the previous paragraph, the quasar mode is accompanied by a significant amount of star formation, especially if the system is to remain consistent with the Magorrian relation. Assuming a ratio of a few hundred for $\Delta M_{bulge}/\Delta M_{BH}$ implies $\sim 10^{11}$ $M_\odot$ of newly formed stars in this system; we call this the *young component*.

In this section, we study what $\sim 10^{11}$ $M_\odot$ of newly formed stars implies about the spatial distribution and age of the young component necessary to be consistent with the observed surface brightness profile and colour of MS0735. We further investigate whether the spatial distribution and the age of the young component are in agreement with general expectations from simulations and observational studies. This exercise checks whether an assumed ratio of a few hundred for $\Delta M_{bulge}/\Delta M_{BH}$ is acceptable for this system.

4.1 Light from the Young Stellar Component

To investigate the spatial distribution and the age of the young component, we should find what fraction of the total stellar light is emitted by the newly formed stars. The following is our method to do so.

First we define our basic set up for star formation. We assume that the total stellar mass consists of two components, a very old red component and a young, recently formed blue component. Also, we assume that the young component has been formed instantaneously. The old and young component are set to form at t_{oc} and t_{yc} before the observed time at the MS0735 redshift of 0.216 (around ~ 2.6 Gyr ago), respectively. In other words, t_{oc} and t_{yc} are the age of the old and young components at the time of the observation, respectively. We assume the old component has formed at the redshift of $z = 6$ (around 12.6 Gyr ago) which implies a $t_{oc} \sim 10$ Gyr. Also, as a framework, we consider the mass of the young component to be 10^{11} $M_\odot$ based on our results from previous sections.

Now, we find the total stellar mass. Donahue et al. (2011) have used data from the Infrared Spectrograph on board the Spitzer Space Telescope to estimate the total stellar mass of MS0735. They end up with around 9.7×10^{11} $M_\odot$ of total stellar mass for this system. On the other hand, one can find a total stellar mass of around 7×10^{11} $M_\odot$ using the absolute K_s-band magnitude $M_K = -26.37$ given by Rafferty

et al. (2006), and a mass to light ratio of around 1 for this passband[1]. However, Schombert (2011) has suggested (also see Lauer et al., 2007) that there can be a systematic bias in 2MASS (2 Micron All Sky Survey) data that underestimates the luminosity by 10 to 40%. Therefore, we choose the Donahue et al. value for the total stellar mass, which also results in a smaller fraction of new star formation. Using the Donahue et al. value, 10^{11} $M_\odot$ of young stars corresponds to $\sim 10\%$ of the total stellar mass.

Next, we use the surface brightness profile of this object in I-band given by McNamara et al. (2009) to find the total amount of light. They fit a Nuker profile to this object:

$$I(r) = I_0(r/r_b)^{-\gamma}(1 + [r/r_b]^{\alpha})^{(\gamma-\beta)/\alpha}. \tag{4.1}$$

The break radius, r_b, is $\sim 1.1 \pm 0.2$ arcsec for this object. The parameters γ, β and α are 0.00 ± 0.02, 2.02 ± 0.04 and 0.99 ± 0.04, respectively. While the end of usable data for I-band is about 18" from the center of the object (McNamara et al., 2009), we extrapolate the Nuker profile up to 25" which is the suggested boundary for this system based on 2MASS $K_s -$ band data. We integrate this Nuker profile, and find the total light in the I-band to be $\sim 7.5 \times 10^{11}$ $L_\odot$. If one assumes the same stellar mass to I-band light ratio (M_*/L_I) for both old and young stars, the corresponding light for the young component should be around 7.5×10^{10} $L_\odot$ in this passband (i.e. 10% of the total light). However, the M_*/L_I varies for stellar populations at different ages (e.g. Maraston, 2005). To find the dependence of M_*/L_I on age, we use Stellar Population Synthesis (SPS) codes.

A SPS code is a package containing libraries of stellar evolutionary sequences and stellar spectra that can be used to compute the spectrum of a stellar population. We present our results using Flexible Stellar Population Synthesis (FSPS; Conroy et al., 2009; Conroy & Gunn, 2010). FSPS, as suggested by its name, has the advantage of being flexible with changeable parameters, and makes it possible to investigate the effects of uncertain physics in stellar evolution. The main variable parameters of FSPS are stellar metallicity[2] (Z), the fraction of blue Horizontal Branch (HB) stars[3]

[1]A passband is the range of frequencies or wavelengths that can pass through a filter without being attenuated. The effective wavelength for K_s-band filter is around 2.17 μm.

[2]In astronomy, the metallicity of an object is the proportion of its matter made up of chemical elements other than hydrogen and helium.

[3]Horizontal Branch star is a star which is undergoing helium fusion in its core and hydrogen fusion in a shell surrounding the core.

(f_{BHB}), the specific frequency of Blue Stragglers (BS) stars[4] (S_{BS}), and the shift in $log(T_{eff})$ and $log(L_{bol})$ along the thermally pulsing AGB[5] (TP-AGB) stars (Δ_T and Δ_L, respectively) where T_{eff} and L_{bol} are the effective temperature and bolometric luminosity of TP-AGB stars. Moreover, various initial mass functions[6] (IMF) can be chosen using FSPS.

We assume a Salpeter IMF[7] for our basic set up. We also use the suggested standard value of zero by FSPS for f_{BHB}, S_{BS}, Δ_T and Δ_L. Extinction corrections have been done using the suggested average hydrogen column density, N_H, from McNamara et al. (2009) for MS0735 and the Cardelli et al. (1989) relation. The only quantity that is left to be set is metallicity (Z). Donahue et al. (2011) reported that they could not distinguish between a $Z/Z_\odot = 1$ or 2 for this system ($Z_\odot$ is the metallicity of Sun). Thus, we use BaSTI isochrones and the BaSel spectral library in the FSPS to do calculations for both metallicities (see the FSPS manual for more details).

For a given fixed stellar mass, the black solid line in Figure 4.1 shows the dependence of M_*/L_I on age for $Z/Z_\odot = 2$. The y-axis is the I-band M_*/L_I ratio of a stellar population at different ages which is scaled by M_*/L_I of an old stellar population with the age of $\sim$ 10 Gyr (This is same as the t_{oc} in our basic set up). The x-axis shows the corresponding age of the stellar population. This plot clearly shows that younger populations are generally brighter. With the scaled values of M_*/L_I, one can calculate what fraction of the total light the young population would emit in I-band ($L_{I,yc}/L_{I,tot}$) at different ages, given that the mass of young population is $\sim$ 10% of the total mass. The blue dashed line in Figure 4.1 shows the corresponding fraction at different ages. Note that the corresponding results for $Z/Z_\odot = 1$ and 2 are very close, thus we do not display the case of $Z/Z_\odot = 1$ in Figure 4.1 for the sake of clarity.

We use these results in the next section and find a reasonable estimate for the smallest possible spatial distribution of the young component at different ages.

[4]Blue Stragglers are unusually hot and bright stars that are usually found in the cores of star clusters.

[5]AGB stars are low to intermediate mass stars ($0.6 - 10$ solar masses) late in their lives.

[6]An initial mass function is a function that describes the mass distribution of a population of stars in terms of their initial mass.

[7]A Salpeter IMF suggests that the number of stars with masses in the range M to $M + dM$ within a specified volume of space, is proportional to $M^{-\alpha}$, where α is a dimensionless exponent $\sim$ 2.35.

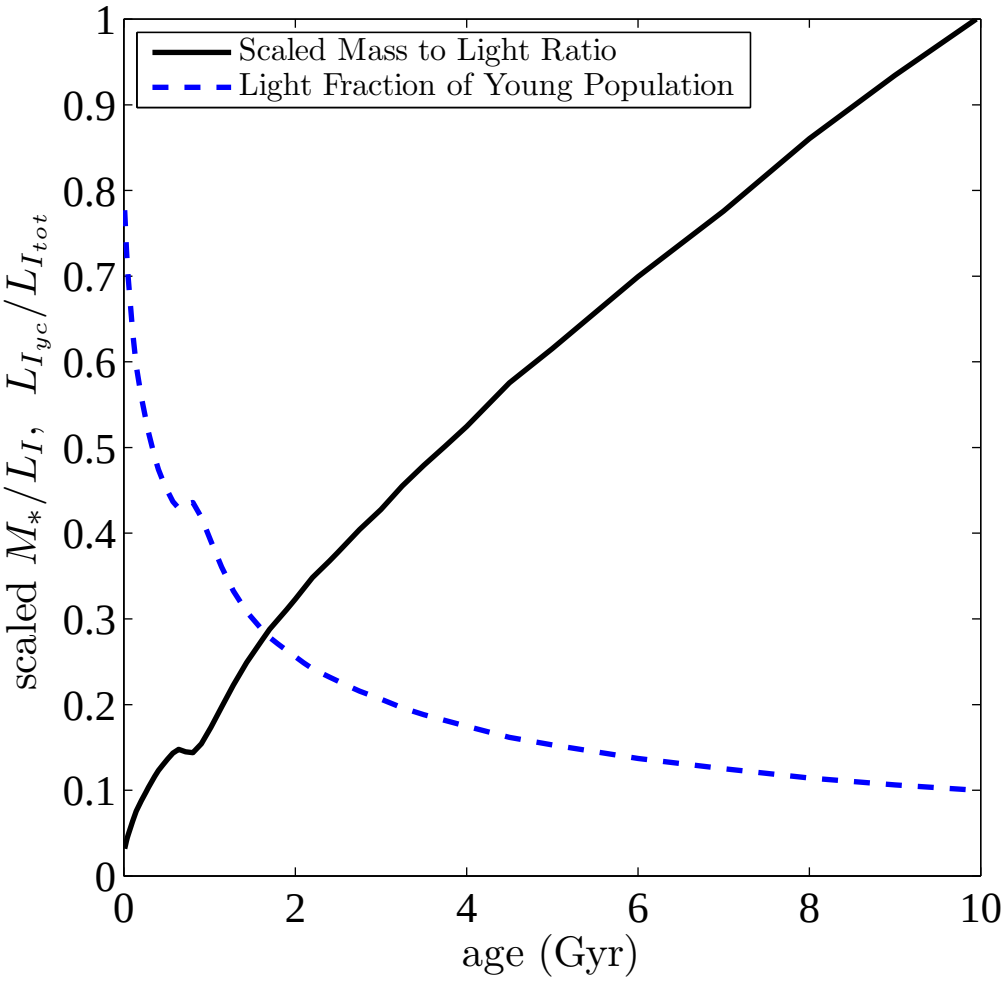

Figure 4.1 The dependence of M_*/L_I and $L_{I,yc}/L_{I,tot}$ on age for $Z/Z_\odot = 2$. For the black solid curve, the y-axis is the M_*/L_I of a stellar population at different ages which is scaled by M_*/L_I of an old stellar population with the age of ~ 10 Gyr (This is same as the t_{oc} in our basic set up). The x-axis shows the corresponding age of the stellar population. Also, for the blue dashed line, the y-axis shows the corresponding fraction of the total I-band light emitting from the young population ($L_{I,yc}/L_{I,tot}$) at different ages, given that the mass of young population is $\sim 10\%$ of the total mass.

4.2 Spatial Distribution of the Young Stellar Component

To find a reasonable estimate for the smallest possible spatial distribution of the young component, we assume that the distribution of old stars is completely flat in the inner regions and is identical to the Nuker profile in the outer regions (see Figure 4.2). We consider the distribution of the young component to be the difference between this old distribution and the observed Nuker profile. With the light profile, one can calculate the fraction of the total light emitted by the young population. We find the smallest spatial distribution of the young component at different ages when its corresponding light fraction is the same as the expected value calculated in the previous section. Note that a completely flat distribution in the inner region for the old component is an extreme assumption, however, it guarantees the smallest spatial distribution for the young component.

Figure 4.3 shows the results. The y-axis is the effective radius[8] (R_e) of the smallest spatial distribution for the young component and the x-axis shows the corresponding age. The black solid curve shows the results for $Z/Z_\odot = 2$. This plot suggests that generally a larger spatial distribution is required for younger populations. This was expected since younger populations are generally brighter, and thus for a given mass, a younger population corresponds to a higher fraction of the total light.

It has been generally believed that star formation should be centrally concentrated within a few hundred parsecs. However, star formation on the order of a couple thousand parsecs has been suggested recently by both high resolution simulations (e.g. Hopkins et al., 2009a; Bois et al., 2010; Teyssier et al., 2010) and observations (Cullen et al., 2006; Wang et al., 2004). The results of Hopkins et al. (2008, 2009a,b) suggest an effective radius of ~ 2.3 kpc for the 10% of newly formed stars in a system like MS0735 (with a total effective radius of 23 kpc). The horizontal red solid line in Figure 4.3 shows this value. They also report a factor of ~ 2 scatter for their results which suggests a range of $1.2 - 4.6$ kpc for the effective radius of the young component. The corresponding scatter is shown by two horizontal red dashed lines in 4.3. While the effective radius of couple of kpc might be considered as a large spatial distribution, Figure 4.3 suggests that the expected effective radius for cases with smaller age is much larger than the suggested value by Hopkins et al. (2008,

[8]The effective radius is the radius at which one half of the total light of the system is emitted interior to this radius.

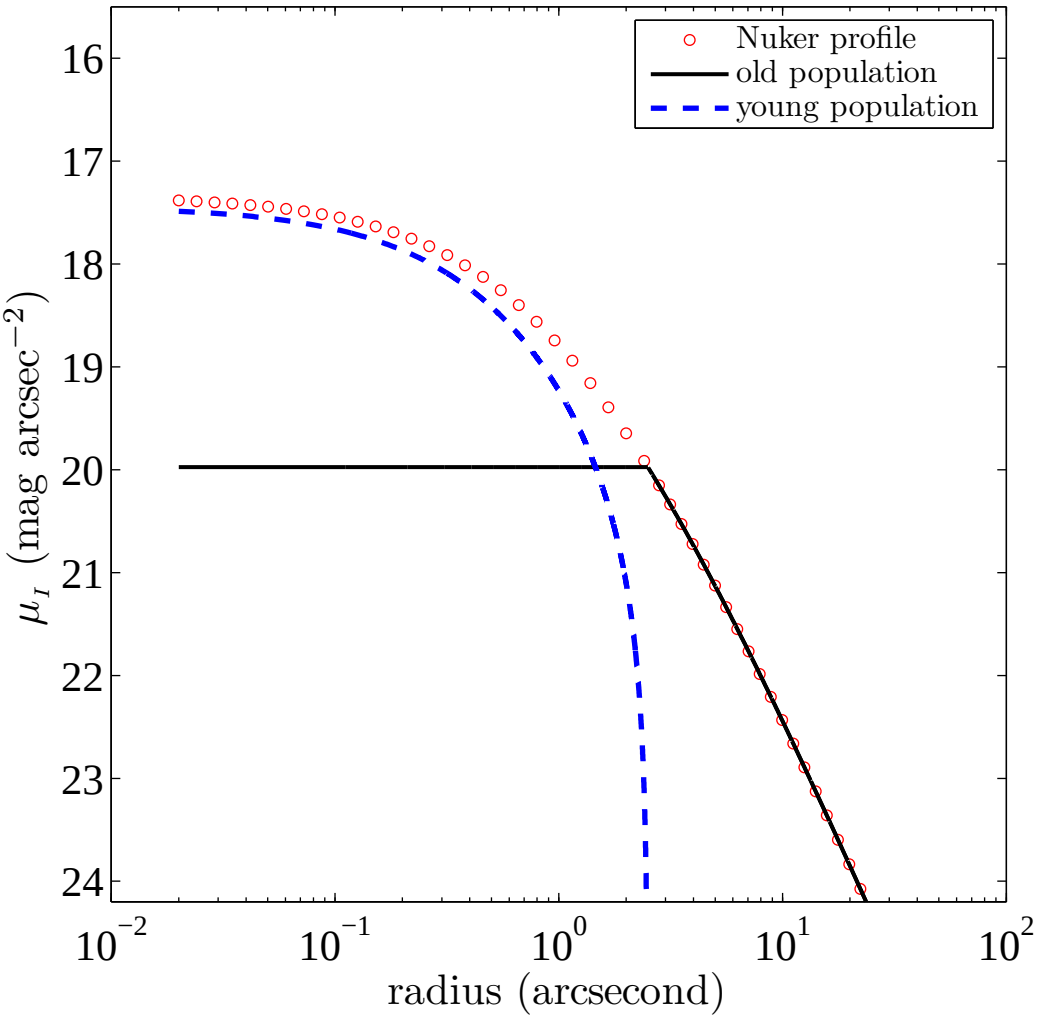

Figure 4.2 I-band surface brightness profile vs. radius. The black solid curve corresponds to the assumed distribution of the old population needed to find the lower limit for the spatial distribution of the young component. The red circles show the observed Nuker profile. As can be seen in the figure, the black solid curve is completely flat in the inner regions and is identical to the Nuker profile in the outer regions. The blue dashed line is the difference between the Nuker profile and the black solid curve, and shows the smallest spatial distribution for the young component.

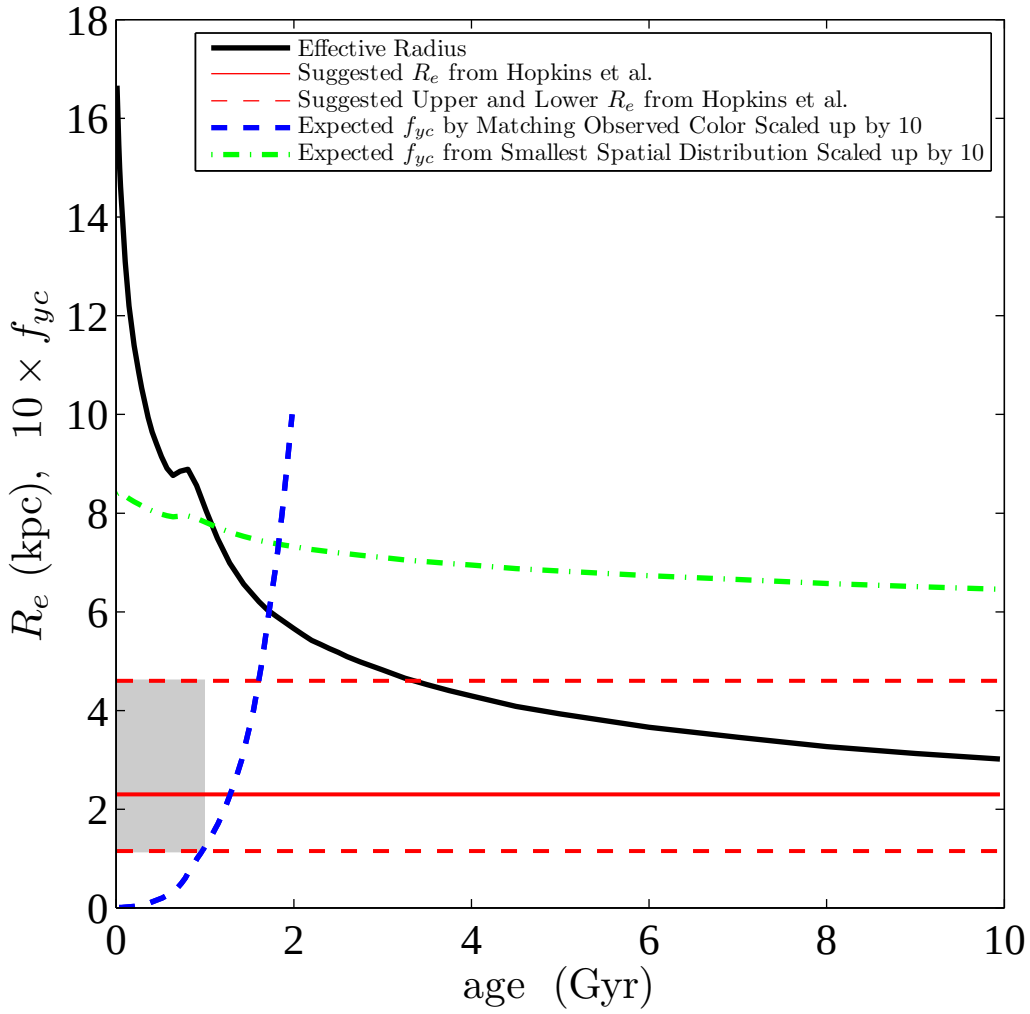

Figure 4.3 Effective radius (R_e) and expected f_{yc} vs. age. For the black solid curve, the y-axis is the R_e of the smallest spatial distribution for the young component and the x-axis shows the corresponding age. The horizontal red solid and dashed lines correspond to the suggested R_e from Hopkins et al. (2008, 2009a,b) and its scatter, respectively. For the blue dashed and green dotted-dashed curves, the y-axis is the expected $10 \times f_{yc}$. The blue dashed curve is the expected f_{yc} vs. t_{yc} in order to match the observed UV-I colour. The green dotted-dashed curve is the expected f_{yc} vs. t_{yc} found from the smallest spatial distributions. Note that the f_{yc} values are scaled up by a factor of 10 for the sake of clarity.

2009a,b).

4.3 Age of the Young Stellar Component

In our basic set up for star formation, we consider a two component stellar population, a very old red component and a young, blue component. When an actual observed colour within an aperture is available, one can use FSPS to determine how long before the observation time (t_{yc}) a given mass fraction of the young component within that aperture (f_{yc}) must have formed in order to match the observed colour. Note that f_{yc} is the mass fraction of the young component within the assumed aperture, and not the total mass fraction of the young component (which is $\sim 10\%$). In this section, we use FSPS and find the required t_{yc} and f_{yc} in order to match the observed UV-I colour of MS0735.

The observational data for I-band have been taken from McNamara et al. (2009). The I-band image from Hubble Space Telescope's Advanced Camera for Surveys (ACS) with the F850LP filter (with angular resolution of 0.05" per pixel) has been used together with a UV image from XMM-Newton's Optical Monitor Wide 1 (W1 - 291 nm) to evaluate the UV-I colour of this cluster for different aperture choices. The aperture size should be small enough to contain the region where the majority of the star formation occurs. However, due to the limitations on pixel size and signal to noise ratio, the aperture cannot be any arbitrarily small size. We consider an aperture size of 1.5", which corresponds to a radius of ~ 5.25 kpc at the redshift of MS0735 ($z = 0.216$). The corresponding observed UV-I colour for this aperture is $\sim 5.74^{+0.32}_{-0.25}$ (the observed colour has been corrected for Galactic extinction).

As has been mentioned, we use FSPS to find the required t_{yc} and f_{yc} in order to match the observed UV-I colour. Our basic set up for FSPS is the same as in the previous section. Note that since we consider a two component stellar population (a very old red component and a young blue component), and also assume an instantaneous burst for the young component, we find a lower limit for the t_{yc}. Any correction to a more realistic star formation history increases the required age of the young component.

Figure 4.4 shows the results of our calculation for $Z/Z_{\odot} = 2$. The y-axis is UV-I colour and the x-axis is t_{yc}. Each curve from left (red) to right (blue) corresponds to a different fraction of the young stellar component (f_{yc}). This plot shows the expected colour for a particular choice of f_{yc} at different assumed t_{yc}. The horizontal black solid

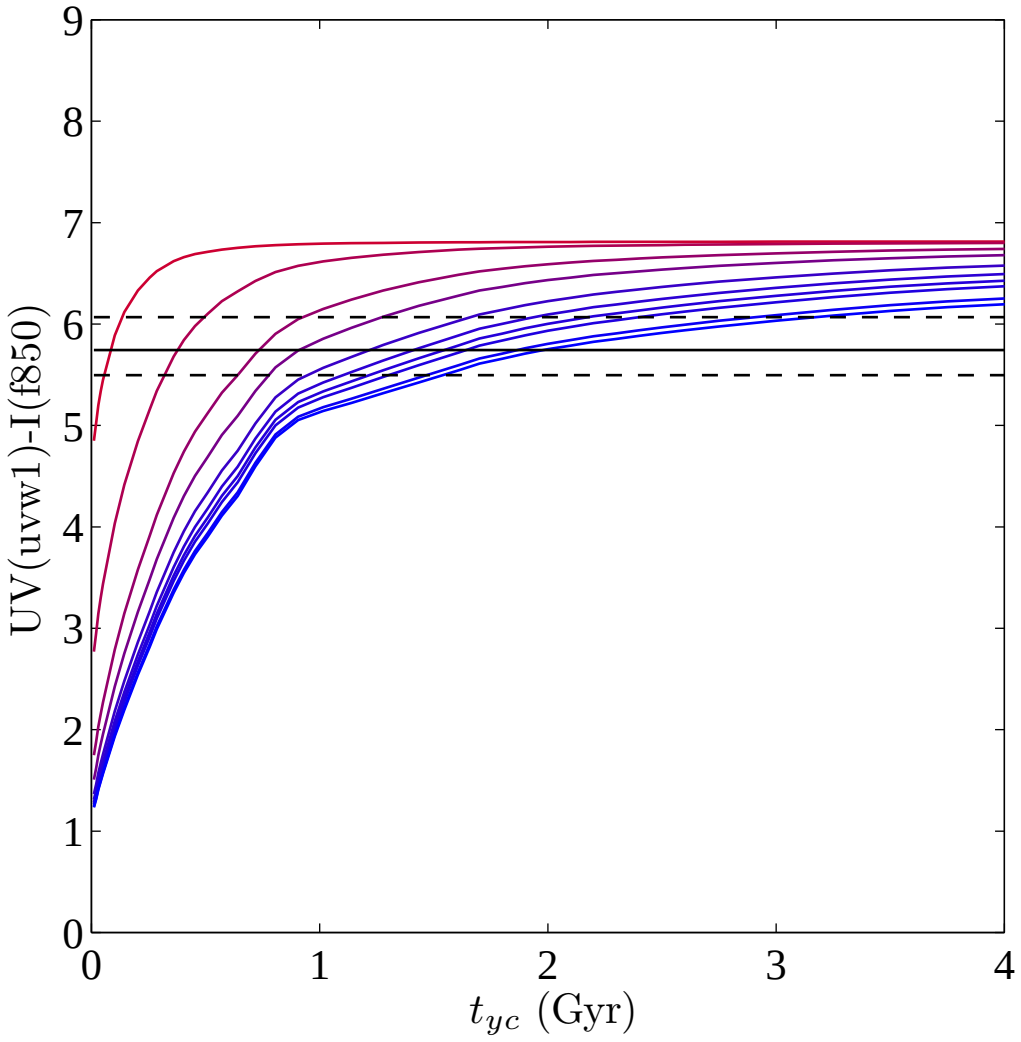

Figure 4.4 $UV(uvw1)$ - $I(f850)$ colour vs. t_{yc} for $Z/Z_{\odot} = 2$. Each left to right (red to blue) curve corresponds to a different fraction of the young stellar component (f_{yc}). Curves correspond to f_{yc} of 0.001, 0.01, 0.05, 0.1, 0.2, 0.3, 0.4, 0.5, 0.8 and 1 from left to right, respectively. The horizontal black solid and dashed lines correspond to the observed colour and its errors. The intersection of the horizontal solid line with different curves shows, for a particular choice of f_{yc}, how long before the observation the star burst must have happened (t_{yc}) in order to matched the actual observed colour at the time of the observation.

and dashed lines correspond to the actual observed colour and errors, respectively. Thus, the intersection of the horizontal solid line with different curves shows, for a particular choice of f_{yc}, how long before the observation the star burst must have happened (t_{yc}) in order to matched the actual observed colour at the time of the observation. We also plot these values of f_{yc} and t_{yc} in Figure 4.3. The blue dashed line shows the results. Note that the f_{yc} values in Figure 4.3 are scaled up by a factor of 10 for the sake of clarity.

4.4 Another Constraint on f_{yc} and t_{yc}

One can also put another constraint on f_{yc} and t_{yc} using our results for the smallest spatial distributions. We found that the size of the smallest young stellar population depends on the stellar age. We can also calculate the corresponding fraction of young stars within 1.5" (our assumed colour aperture size) as a function of stellar age. We plot the results in Figure 4.3 as the green dotted-dashed line. The intersection of this line and the blue dashed line in Figure 4.3 (which is the constraint on f_{yc} and t_{yc} coming from the actual observed colour), gives us the required t_{yc} of the young stellar component for cases with the smallest spatial distribution. One can also easily find the corresponding effective radius from the black solid curve in Figure 4.3 with the value of t_{yc}. For the case of $Z/Z_{\odot} = 2$, the corresponding t_{yc} and R_e are 1.8 Gyr and 5.9 kpc, respectively. If one considers the lower limit of the observed colour in Figure 4.4, the corresponding t_{yc} and R_e become 1.5 Gyr and 6.5 kpc. Also, considering the upper limit on the observed colour in Figure 4.4 suggests a t_{yc} and R_e of 2.8 Gyr and 5 kpc. Altogether, as can easily be seen from the black solid curve in Figure 4.3, a smaller spatial distribution requires a larger t_{yc} and vice versa.

4.5 Changing Parameters in FSPS

We also performed similar exercises by changing different parameters in the FSPS. We studied cases with different IMFs (for instance see Figure 4.5 for a case with Chabrier IMF and $Z/Z_{\odot} = 2$); however, the corresponding t_{yc} and R_e curves (the blue dashed and black solid lines in Figure 4.3 and 4.5) did not change significantly. For a case with Chabrier IMF and $Z/Z_{\odot} = 2$, the required t_{yc} and R_e are 1.9 Gyr and 6.1 kpc, respectively. A non zero fraction of blue Horizontal Branch (HB) stars or specific frequency of Blue Stragglers (BS) stars does not significantly change the

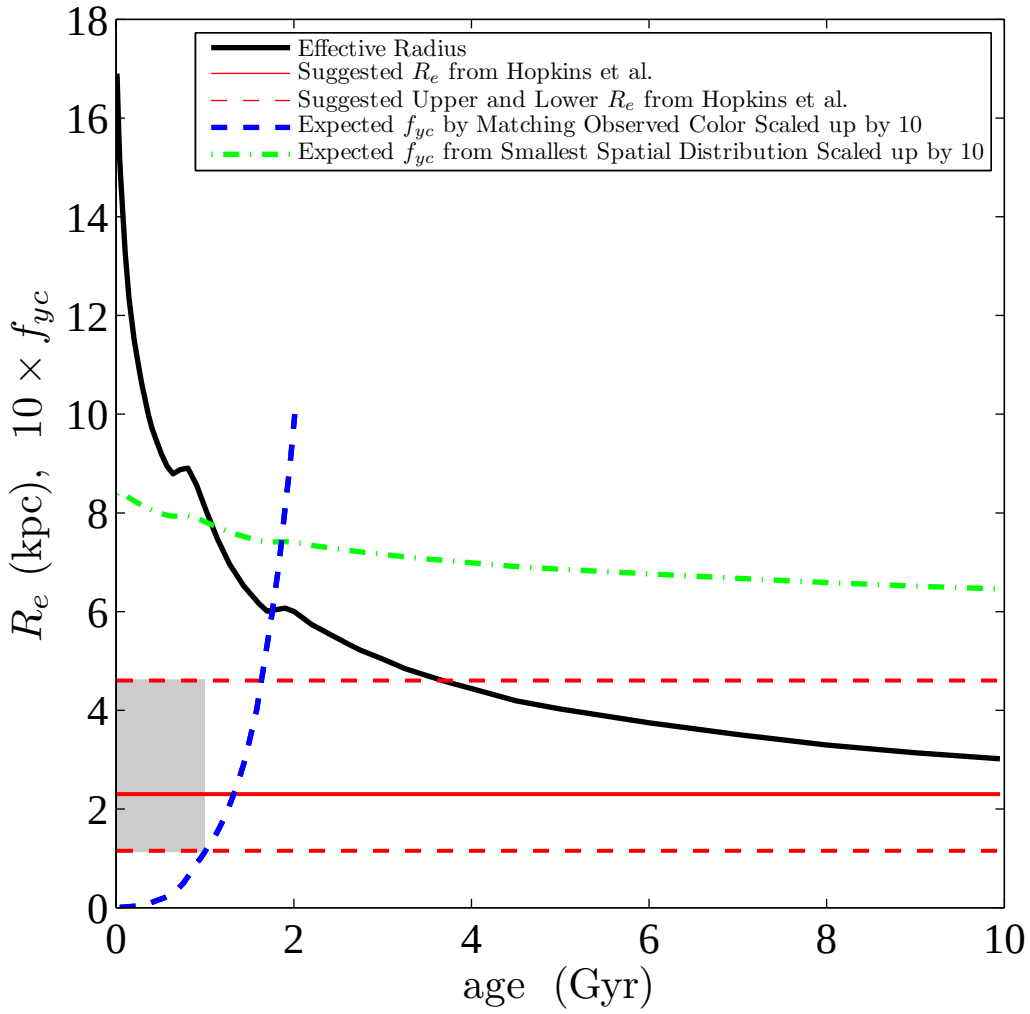

Figure 4.5 Effective radius (R_e) and expected f_{yc} vs. age for $Z/Z_\odot = 2$ and Chabrier IMF. This Figure is similar to Figure 4.3 but for a Chabrier IMF. For the black solid curve, the y-axis is the R_e of the smallest spatial distribution for the young component and the x-axis shows the corresponding age. The horizontal red solid and dashed lines correspond to the suggested R_e from Hopkins et al. (2008, 2009a,b) and its scatter, respectively. For the blue dashed and green dotted-dashed curves, the y-axis is the expected $10 \times f_{yc}$. The blue dashed curve is the expected f_{yc} vs. t_{yc} in order to match the observed UV-I colour. The green dotted-dashed curve is the expected f_{yc} vs. t_{yc} found from the smallest spatial distributions. Note that the f_{yc} values are scaled up by a factor of 10 for the sake of clarity.

corresponding R_e curve, though, it increases the required t_{yc} by changing the observed colour. Generally, a non zero fraction of blue Horizontal Branch (HB) stars or specific frequency of Blue Stragglers (BS) stars make the expected colour bluer, and thus a young component requires a larger t_{yc} in order to match observations (since stellar populations become redder as they evolve). Assuming $Z/Z_{\odot} = 1$ also does not make a significant change in the corresponding R_e curve. However, it increases the required t_{yc} since, again, lower metallicity makes the expected UV-I colour bluer.

In FSPS, TP-AGB are parametrized by two changeable parameters of Δ_T, the shift in $log(T_{eff})$, and Δ_L, the shift in $log(L_{bol})$, where T_{eff} and L_{bol} are the effective temperature and bolometric luminosity of TP-AGB stars. We considered different combination of these two parameters, and in one of the very extreme cases, we set Δ_T and Δ_T to the highest allowed values of 0.2 and 0.4, respectively. The results for this case with $Z/Z_{\odot} = 2$ are shown in Figure 4.6. The corresponding t_{yc} and R_e are 1.5 Gyr and 7.4 kpc, respectively. Generally, the corresponding R_e curve is shifted to the higher values and the required t_{yc} is decreased. The corresponding R_e curve shifts to the higher values because the scaled M_*/L_I is smaller for this case, and the young component corresponds to a larger fraction of the total light of the object. Thus, a larger spatial distribution is needed. Also, the required t_{yc} decreases since a pronounced effect of TP-AGB stars makes the expected UV-I colour redder. Thus, the actual observed colour can be matched with a younger recently formed population.

One might also change the star formation history, for instance by assuming a smaller t_{oc} (the age of the old component) in order to decrease the scaled M_*/L_I ratio, and thus, decrease the expected R_e. However, any change in the star formation history makes the the expected colour bluer, and thus, increases the required t_{yc}.

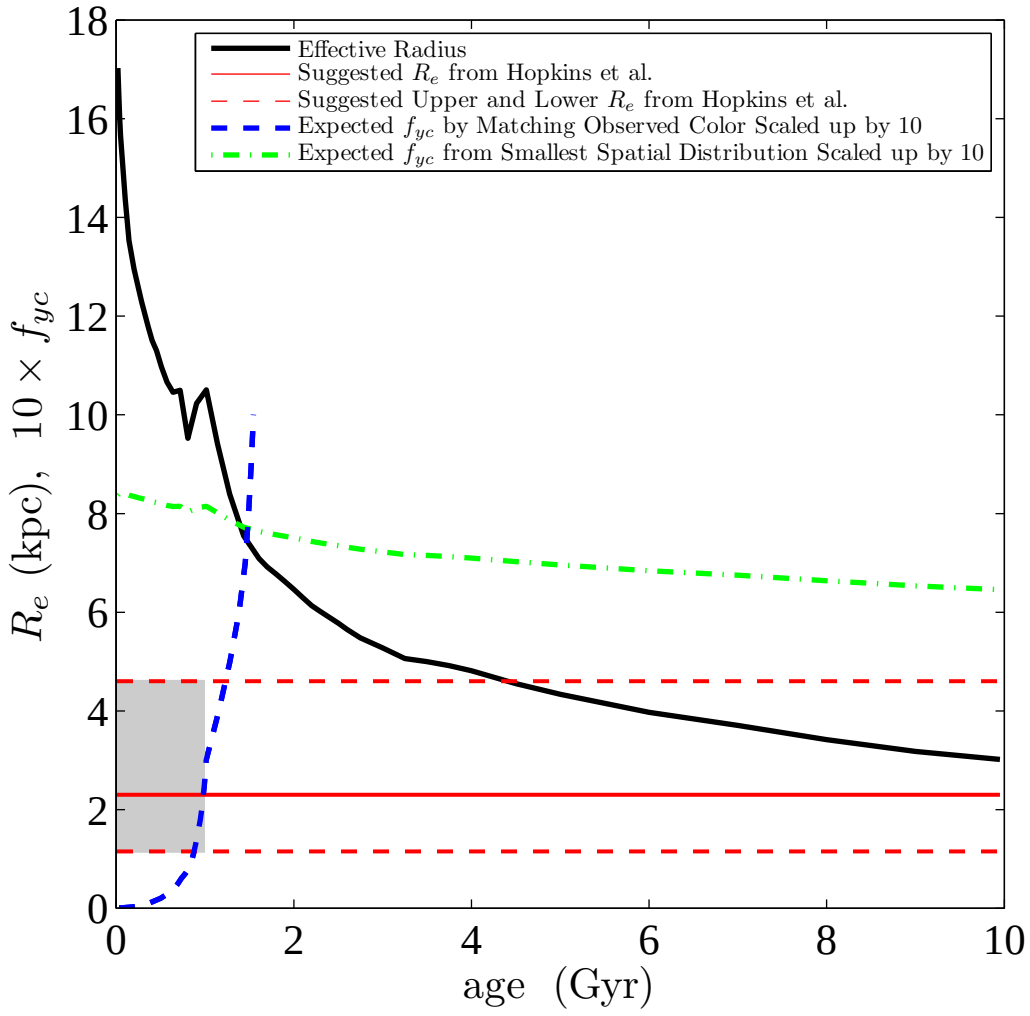

Figure 4.6 Effective radius (R_e) and expected f_{yc} vs. age for $Z/Z_\odot = 2$, $\Delta_T = 0.2$ and $\Delta_L = 0.4$. This Figure is similar to Figure 4.3 but for $\Delta_T = 0.2$ and $\Delta_L = 0.4$. For the black solid curve, the y-axis is the R_e of the smallest spatial distribution for the young component and the x-axis shows the corresponding age. The horizontal red solid and dashed lines correspond to the suggested R_e from Hopkins et al. (2008, 2009a,b) and its scatter, respectively. For the blue dashed and green dotted-dashed curves, the y-axis is the expected $10 \times f_{yc}$. The blue dashed curve is the expected f_{yc} vs. t_{yc} in order to match the observed UV-I colour. The green dotted-dashed curve is the expected f_{yc} vs. t_{yc} found from the smallest spatial distributions. Note that the f_{yc} values are scaled up by a factor of 10 for the sake of clarity.

Chapter 5

Discussion

5.1 What Do Our Results Imply?

Simulations have shown that there is a delay between the peak of SFR inside of a given annulus and the peak of AGN activity (e.g. Hopkins, 2012). This delay varies from 10^7 yr on small scales (10 pc) to a few $\sim 10^8$ yr on kpc scales (Hopkins, 2012). Moreover, the lifetime of a quasar mode has been found to be on the order of $\sim 10^8$ yr. These results suggest that a time window between the formation of the young component and the end of the ADAF mode in our scenario, which is the same as t_{yc}, should be at the order of $\sim 10^8$ yr. In other words, a period of 1 Gyr can be considered to be an upper limit for this time window (which includes the delay, quasar mode and ADAF mode). Combining this constraint on t_{yc} with the results of the Hopkins et al. (2008, 2009a,b) gives the shaded region in Figure 4.3 as the accepted parameter space. Comparing our results with the accepted parameter space suggests that a very high amount of star formation is unlikely to be present in this system. This is not in agreement with the usual interpretation of the Magorrian relation with an assumed ratio of a few hundred for $\Delta M_{bulge}/\Delta M_{BH}$.

One should note that the above result is for cases where the BHs have to be spun up. However, cases with ultra massive BHs do not need to be spun up in order to produce a sufficiently energetic outburst. Thus, there is no need of a quasar mode with a coupled SF. As a result, our calculations suggest that for all intents and purposes, the existence of an ultra massive BH ($M_{BH,f} \sim 2 \times 10^{10}$ $M_\odot$ or larger for this object) is the simplest solution.

5.2 Systematic Effects

Benson & Babul (2009) have done their calculation of the ADAF mode for two different values for the dimensionless specific energy (E_{ADAF}) of accreted material; they use an ideal ADAF value as well as a thin-disk value as suggested by simulations. In an ideal unmagnetized ADAF, the gas starts out cold at large radii and all dissipated energy is advected along with the flow. The dimensionless specific energy of the accreted material is $E_{ADAF} \sim 1$ for this case, and the specific angular momentum of the accreted gas is typically sub-Keplerian[1]. On the other hand, recent simulations have suggested that when the effect of magnetic field is considered, and less constrained flow are allowed to be explored, the angular momentum is typically less than the thin disk, but the energy of the accreted material is in fact close to the thin disk ($E_{ADAF} = E_{ISCO}$). In this paper, we have presented results for $E_{ADAF} \sim 1$, however, we have done our calculation for both models. Assuming $E_{ADAF} = E_{ISCO}$ does not change our results significantly, and the required gas in the accretion disk around the BH is still at the same order. However, since $E_{ADAF} = E_{ISCO}$ has a slightly higher equilibrium spin with a slightly higher jet efficiency of ~ 0.18, the smallest M_{BH} which is able to produce enough power and energy and satisfy our constraints without needing to be spun up decreases to $M_{BH,f} \sim 1.5 \times 10^{10}$ $M_\odot$ (rather than $M_{BH,f} \sim 2.1 \times 10^{10}$ $M_\odot$ for $E_{ADAF} \sim 1$).

Another uncertainty is the estimation of the total amount of energy that has been produced by the BH during the ADAF mode. The total estimated energy is the sum of two components: the energy of the induced shock to the ambient material as a result of lobe formation, and the enthalpy[2] of the cavities. McNamara et al. (2009) argue that the shock energy of MS0735 (5.7×10^{61} erg) has been underestimated, so 1.21×10^{62} erg can be considered as a lower estimation for the total amount of the outburst energy. Any correction to higher energies pushes the required amount of gas in the accretion disk around the BH to even higher values. However, there can also be some uncertainties in the estimate of the other part of the total energy. Rafferty et al. (2006) have used a standard model of purely hydrodynamic expansion in order to estimate the enthalpy of the cavities. Although this is the standard method that

[1]Gas can lose part of its angular momentum before it brings itself together to form an accretion disk. This can result in a sub-Keplerian accretion.

[2]Enthalpy is a measure of the total energy of a thermodynamic system. It includes the internal energy, which is the energy required to create a system, and the amount of energy required to make room for it by displacing its environment and establishing its volume and pressure.

is often used in the literature, Diehl et al. (2008) have shown that it might not be the correct model since the evolution of the size of the observed cavities is not consistent with the prediction of this standard model. Thus, if the estimate of the energy in the cavities can be different, the total amount of the energy produced by the BH can also change. If a model predicts a higher energy for cavities, it again results in a higher amount of required gas in the accretion disk around the BH. However, if one could end up with a lower amount of energy, the required amount of gas in the accretion disk around the BH could potentially be pushed to lower values. As an extreme case, we have done our calculation again, neglecting the enthalpy of the cavities. Since the shock energy and the enthalpy of the cavities are close to each other for this system, the total amount of the energy should be decreased by a factor of two. We found that even this extreme assumption cannot decrease the required gas in the accretion disk around the BH and the smallest M_{BH} which can produce a sufficiently energetic outburst without needing to be spun up by more than a factor of about two. Thus, as long as the estimated energy for enthalpy and shock are on the same order that have been found, our conclusion remains unchanged. This is also true if these gigantic lobes could be considered as several smaller lobes, similar to what has been found for Hydra A (Wise et al., 2007). In this case, the order of the total energy most likely remains unchanged, and the total energy will be close to the energy of the largest lobe, which is usually formed first and is farthest from the centre. So, while a more detailed picture is required, one can consider the formation of the first and largest pair of lobes, and use a similar method to study the system to the first order.

Altogether, as long as a different model does not predict a total estimated energy that is much smaller, our conclusion remains robust. However, such a model would most likely result in a decreased calculated energy for *all* systems which implies a lower importance for AGNs than is currently believed.

Chapter 6

Summary

In this work, we have studied the galaxy cluster MS0735.6+7421 that hosts the most energetic observed AGN outburst so far. The total energy of the outburst is around 1.21×10^{62} erg with an age of 1.1×10^8 yr (McNamara et al., 2009).

Assuming an efficiency of ~ 0.13 (the corresponding efficiency for the equilibrium spin), the required accretion rate during a period of 1.1×10^8 yr of ADAF mode must be ~ 4.6 $M_\odot$ yr^{-1} in order to explain the AGN burst in MS0735. For $M_{BH,f} \geq 2.1 \times 10^{10}$ $M_\odot$, this accretion rate is comfortably below the critical threshold of ~ 0.01 of the Eddington accretion rate and the jet outburst can be attributed to mass accretion via an ADAF. However, for the suggested BH mass of 2×10^9 $M_\odot$ or 5×10^9 $M_\odot$ for MS0735 (Rafferty et al., 2006; McNamara et al., 2009), the required accretion rate exceeds the critical threshold of ~ 0.01 of the Eddington accretion rate, and the AGN cannot be in an ADAF mode during the burst. To maintain an ADAF mode during the radio outburst, McNamara et al. (2011) have proposed that the BH must have been spun up to near maximal spins at the start of the outburst.

There are two ways to increase the BH spin: one is via gas accretion, and the other is via a merger with another BH. We explored these mechanisms to spin up the BH and investigated possible solutions that can explain the AGN outburst in this system. We showed that regardless of how one spins up the BH, i.e. via a pure gas accretion or BH-BH merger scenario, the process requires at least a few times 10^8 $M_\odot$ of gas in the accretion disk around the BH.

Moreover, the AGN should be in the quasar mode during the spin-up phase since jet formation should not start until the BH spin is high enough. While there is evidence that a considerable amount of SF does not always accompany the radio (ADAF) mode (e.g. Tadhunter et al., 2007), the quasar mode is accompanied by a

significant amount of star formation. Considering this point, one might interpret the observed $M_{BH} - M_{bulge}$ scaling relation in the local universe (Magorrian relation) as the co-evolution of M_{BH} and M_{bulge} with a ratio of a few hundred for $\Delta M_{bulge}/\Delta M_{BH}$ during quasar mode. However, assuming a ratio of a few hundred for $\Delta M_{bulge}/\Delta M_{BH}$ implies $\sim 10^{11}$ $M_{\odot}$ of newly formed stars in MS0735.

We further studied what $\sim 10^{11}$ $M_{\odot}$ of newly formed stars implies about the spatial distribution and age of the young component necessary to be consistent with the observed surface brightness profile and colour of MS0735. Figure 4.3 shows the results. This plot suggests that the required spatial distribution for the newly formed stars is consistent with the general expectations from simulations only when the age of the newly formed stars is larger than a couple of Gyr. However, this value is much larger than what is expected for the time window between the SF and end of the AGN activity (Hopkins, 2012). Altogether, comparing our results with the accepted parameter space (the shaded region in Figure 4.3) suggests that a very high amount of star formation is unlikely to be present in this system. This is not in agreement with the usual interpretation of the Magorrian relation with an assumed ratio of a few hundred for $\Delta M_{bulge}/\Delta M_{BH}$.

One should note that the above result is for cases where the BHs have to be spun up. However, cases with ultra massive BHs do not need to be spun up in order to produce a sufficiently energetic outburst. Thus, there is no need of a quasar mode with a coupled SF. As a result, our calculations suggest that for all intents and purposes, the existence of an ultra massive BH ($M_{BH,f} \sim 2 \times 10^{10}$ $M_{\odot}$ or larger for this object) is the simplest solution.

Bibliography

Agol, E. & Krolik, J. H. 2000, Astrophysical Journal, 528, 161

Allen, S. W., Dunn, R. J. H., Fabian, A. C., Taylor, G. B., & Reynolds, C. S. 2006, Monthly Notices of the RAS, 372, 21

Armitage, P. J. & Natarajan, P. 2002, Astrophysical Journal, Letters to the Editor, 567, L9

Baldry, I. K., Glazebrook, K., Brinkmann, J., Ivezić, Ž., Lupton, R. H., Nichol, R. C., & Szalay, A. S. 2004, Astrophysical Journal, 600, 681

Bardeen, J. M. 1970, Nature, 226, 64

Begelman, M. C., Blandford, R. D., & Rees, M. J. 1980, Nature, 287, 307

Bennett, A. S. 1962, MmRAS, 68, 163

Benson, A. J. & Babul, A. 2009, Monthly Notices of the RAS, 397, 1302

Bildfell, C., Hoekstra, H., Babul, A., & Mahdavi, A. 2008, Monthly Notices of the RAS, 389, 1637

Bîrzan, L., Rafferty, D. A., McNamara, B. R., Wise, M. W., & Nulsen, P. E. J. 2004, Astrophysical Journal, 607, 800

Blandford, R. D. & Znajek, R. L. 1977, Monthly Notices of the RAS, 179, 433

Blanton, E. L., Sarazin, C. L., McNamara, B. R., & Wise, M. W. 2001, Astrophysical Journal, Letters to the Editor, 558, L15

Bogdanović, T., Reynolds, C. S., & Miller, M. C. 2007, Astrophysical Journal, Letters to the Editor, 661, L147

Bois, M. et al. 2010, Monthly Notices of the RAS, 406, 2405

Bondi, H. 1952, Monthly Notices of the RAS, 112, 195

Burbidge, G. R., Burbidge, E. M., & Sandage, A. R. 1963, Reviews of Modern Physics, 35, 947

Cardelli, J. A., Clayton, G. C., & Mathis, J. S. 1989, Astrophysical Journal, 345, 245

Carroll, B. W. & Ostlie, D. A. 2007, An Introduction to Moderin Astrophysics (Addison-Wesley)

Chandrasekhar, S. 1943, Astrophysical Journal, 97, 255

Churazov, E., Sazonov, S., Sunyaev, R., Forman, W., Jones, C., & Böhringer, H. 2005, Monthly Notices of the RAS, 363, L91

Conroy, C. & Gunn, J. E. 2010, Astrophysical Journal, 712, 833

Conroy, C., Gunn, J. E., & White, M. 2009, Astrophysical Journal, 699, 486

Cowie, L. L. & Binney, J. 1977, Astrophysical Journal, 215, 723

Croston, J. H., Hardcastle, M. J., Mingo, B., Evans, D. A., Dicken, D., Morganti, R., & Tadhunter, C. N. 2011, Astrophysical Journal, Letters to the Editor, 734, L28

Cuadra, J., Armitage, P. J., Alexander, R. D., & Begelman, M. C. 2009, Monthly Notices of the RAS, 393, 1423

Cullen, H., Alexander, P., & Clemens, M. 2006, Monthly Notices of the RAS, 366, 49

David, L. P., Nulsen, P. E. J., McNamara, B. R., Forman, W., Jones, C., Ponman, T., Robertson, B., & Wise, M. 2001, Astrophysical Journal, 557, 546

Di Matteo, T., Quataert, E., Allen, S. W., Narayan, R., & Fabian, A. C. 2000, Monthly Notices of the RAS, 311, 507

Diehl, S., Li, H., Fryer, C. L., & Rafferty, D. 2008, Astrophysical Journal, 687, 173

Donahue, M., de Messières, G. E., O'Connell, R. W., Voit, G. M., Hoffer, A., McNamara, B. R., & Nulsen, P. E. J. 2011, Astrophysical Journal, 732, 40

Dotti, M., Salvaterra, R., Sesana, A., Colpi, M., & Haardt, F. 2006, Monthly Notices of the RAS, 372, 869

Edge, D. O., Shakeshaft, J. R., McAdam, W. B., Baldwin, J. E., & Archer, S. 1959, MmRAS, 68, 37

Ehman, J. R., Dixon, R. S., & Kraus, J. D. 1970, Astronomical Journal, 75, 351

Ekers, R. D. 1969, Australian Journal of Physics Astrophysical Supplement, 6, 3

Fanidakis, N., Baugh, C. M., Benson, A. J., Bower, R. G., Cole, S., Done, C., & Frenk, C. S. 2011, Monthly Notices of the RAS, 410, 53

Fath, E. A. 1909, Lick Observatory Bulletin, 5, 71

Ferrarese, L. & Merritt, D. 2000, Astrophysical Journal, Letters to the Editor, 539, L9

Gammie, C. F. 1999, Astrophysical Journal, Letters to the Editor, 522, L57

Gammie, C. F., Shapiro, S. L., & McKinney, J. C. 2004, Astrophysical Journal, 602, 312

Gebhardt, K. et al. 2000, Astrophysical Journal, Letters to the Editor, 539, L13

Gower, J. F. R., Scott, P. F., & Wills, D. 1967, MmRAS, 71, 49

Häring, N. & Rix, H.-W. 2004, Astrophysical Journal, Letters to the Editor, 604, L89

Hazard, C., Gulkis, S., & Bray, A. D. 1967, Astrophysical Journal, 148, 669

Hazard, C., Mackey, M. B., & Shimmins, A. J. 1963, Nature, 197, 1037

Hicks, A. K. & Mushotzky, R. 2005, Astrophysical Journal, Letters to the Editor, 635, L9

Hopkins, P. F. 2012, Monthly Notices of the RAS, 420, L8

Hopkins, P. F., Cox, T. J., Dutta, S. N., Hernquist, L., Kormendy, J., & Lauer, T. R. 2009a, Astrophysical Journal, Supplement Series, 181, 135

Hopkins, P. F., Hernquist, L., Cox, T. J., Dutta, S. N., & Rothberg, B. 2008, Astrophysical Journal, 679, 156

Hopkins, P. F., Lauer, T. R., Cox, T. J., Hernquist, L., & Kormendy, J. 2009b, Astrophysical Journal, Supplement Series, 181, 486

Hubble, E. P. 1926, Astrophysical Journal, 64, 321

Ivanov, P. B., Papaloizou, J. C. B., & Polnarev, A. G. 1999, Monthly Notices of the RAS, 307, 79

Johnstone, R. M., Allen, S. W., Fabian, A. C., & Sanders, J. S. 2002, Monthly Notices of the RAS, 336, 299

Kesden, M. 2008, Phys. Rev. D, 78, 084030

King, A. R., Pringle, J. E., & Hofmann, J. A. 2008, Monthly Notices of the RAS, 385, 1621

Kormendy, J. & Richstone, D. 1995, Annual Review of Astronomy and Astrophysics, 33, 581

Krolik, J. H. 1999, Astrophysical Journal, Letters to the Editor, 515, L73

Lauer, T. R. et al. 2007, Astrophysical Journal, 662, 808

Lea, S. M., Silk, J., Kellogg, E., & Murray, S. 1973, Astrophysical Journal, Letters to the Editor, 184, L105

Li, L.-X. 2000, Astrophysical Journal, Letters to the Editor, 533, L115

— 2002, Astrophysical Journal, 567, 463

Livio, M., Ogilvie, G. I., & Pringle, J. E. 1999, Astrophysical Journal, 512, 100

Lodato, G., Nayakshin, S., King, A. R., & Pringle, J. E. 2009, Monthly Notices of the RAS, 398, 1392

Loeb, A. 2007, Physical Review Letters, 99, 041103

Maccarone, T. J., Gallo, E., & Fender, R. 2003, Monthly Notices of the RAS, 345, L19

Magorrian, J. et al. 1998, Astronomical Journal, 115, 2285

Maraston, C. 2005, Monthly Notices of the RAS, 362, 799

Marconi, A. & Hunt, L. K. 2003, Astrophysical Journal, Letters to the Editor, 589, L21

Mathews, W. G. & Bregman, J. N. 1978, Astrophysical Journal, 224, 308

Matthews, T. A. & Sandage, A. R. 1963, Astrophysical Journal, 138, 30

McNamara, B. R., Kazemzadeh, F., Rafferty, D. A., Bîrzan, L., Nulsen, P. E. J., Kirkpatrick, C. C., & Wise, M. W. 2009, Astrophysical Journal, 698, 594

McNamara, B. R., Nulsen, P. E. J., Wise, M. W., Rafferty, D. A., Carilli, C., Sarazin, C. L., & Blanton, E. L. 2005, Nature, 433, 45

McNamara, B. R. et al. 2006, Astrophysical Journal, 648, 164

McNamara, B. R., Rohanizadegan, M., & Nulsen, P. E. J. 2011, Astrophysical Journal, 727, 39

McNamara, B. R. et al. 2000, Astrophysical Journal, Letters to the Editor, 534, L135

Meier, D. L. 2001, Astrophysical Journal, Letters to the Editor, 548, L9

Milosavljević, M. & Merritt, D. 2001, Astrophysical Journal, 563, 34

Milosavljević, M. & Phinney, E. S. 2005, Astrophysical Journal, Letters to the Editor, 622, L93

Miralda-Escudé, J. & Kollmeier, J. A. 2005, Astrophysical Journal, 619, 30

Narayan, R. & Yi, I. 1994, Astrophysical Journal, Letters to the Editor, 428, L13

— 1995, Astrophysical Journal, 452, 710

Nulsen, P. E. J., Hambrick, D. C., McNamara, B. R., Rafferty, D., Birzan, L., Wise, M. W., & David, L. P. 2005, Astrophysical Journal, Letters to the Editor, 625, L9

Perley, R. A., Dreher, J. W., & Cowan, J. J. 1984, Astrophysical Journal, Letters to the Editor, 285, L35

Peterson, J. R., Kahn, S. M., Paerels, F. B. S., Kaastra, J. S., Tamura, T., Bleeker, J. A. M., Ferrigno, C., & Jernigan, J. G. 2003, Astrophysical Journal, 590, 207

Pilkington, J. D. H. & Scott, P. F. 1965, MmRAS, 69, 183

Pipino, A., Kaviraj, S., Bildfell, C., Babul, A., Hoekstra, H., & Silk, J. 2009, Monthly Notices of the RAS, 395, 462

Rafferty, D. A., McNamara, B. R., Nulsen, P. E. J., & Wise, M. W. 2006, Astrophysical Journal, 652, 216

Salim, S. et al. 2007, Astrophysical Journal, Supplement Series, 173, 267

Schombert, J. 2011, ArXiv e-prints

Seyfert, C. K. 1943, Astrophysical Journal, 97, 28

Shakura, N. I. & Sunyaev, R. A. 1973, Astronomy and Astrophysics, 24, 337

Slipher, V. M. 1917, Lowell Observatory Bulletin, 3, 59

Tadhunter, C. et al. 2007, Astrophysical Journal, Letters to the Editor, 661, L13

Teyssier, R., Chapon, D., & Bournaud, F. 2010, Astrophysical Journal, Letters to the Editor, 720, L149

Thorne, K. S. 1974, Astrophysical Journal, 191, 507

Volonteri, M., Sikora, M., & Lasota, J.-P. 2007, Astrophysical Journal, 667, 704

Wang, J.-M. & Hu, C. 2005, Astrophysical Journal, Letters to the Editor, 630, L125

Wang, Z. et al. 2004, Astrophysical Journal, Supplement Series, 154, 193

Wise, M. W., McNamara, B. R., Nulsen, P. E. J., Houck, J. C., & David, L. P. 2007, Astrophysical Journal, 659, 1153

Zel'Dovich, Y. B. 1965, Soviet Astronomy, 9, 221